



OPEN

Study on the forming mechanism and evolutionary pattern of stagnant region in mechanical scratching

Yanchun Ding^{1✉}, Wenxin Yu¹, Guangfeng Shi^{2✉}, Hailong Lv¹, Jiayu Wu¹, Li Mao¹ & Guohong Li¹

In this paper, a combination of theoretical modeling, finite element simulation, and experimental methods is employed to investigate the forming mechanism and evolutionary pattern of the stagnant region during mechanical scratching with a diamond wedge tool. The study is structured as follows: Firstly, a theoretical calculation model for the geometric parameters of the stagnant region on the formed groove surface is established based on the contact friction partition mechanism and slip-line field theory. The model indicates that the geometric parameters l_{B-sgr} , l_{V-sgr} and Δl_{sg} of the stagnant region are determined by the length of the stagnant region l_{p-sg} in the plastic flow plane and the transformation parameters. Secondly, the formation process of the stagnant region in mechanical scratching is investigated using an orthogonal cutting simulation model with a negative rake angle tool. The results reveal that the stagnant region is a plastic deformation region formed due to the geometrical characteristics of the negative front surface of the scratching tool and its excessive extrusion, which leads to the formation of adhesive friction within the material. Thirdly, the characteristics of the stagnant region are determined through scratching experiments. Compared to the material in the plastic flow region, the material within the stagnant region exhibits finer and denser microstructures, reduced surface hardening peaks and hardened layer depths, and significantly improved surface roughness. Finally, the evolutionary pattern of the stagnant region under the influence of scratching processing parameters is examined based on the theoretical calculation model of the geometric parameters and the scratching experiment. The findings indicate that as the wedge angle of the scratching tool decreases, the relief angle increases, the absolute value of the rotation angle around the Y-axis decreases, the scratching speed decreases, and the material's plastic adherence improves, the $P_{I/k}$ value decreases, the l_{p-sg} value increases, and consequently, the geometric parameters l_{B-sgr} , l_{V-sgr} and Δl_{sg} of the stagnant region on the formed groove surface also increase. The deviation analysis of the geometric parameters of the stagnant region reveals a consistent trend between the theoretical and experimental values of l_{V-sg} and Δl_{sg} with maximum deviations of 15 μm and 4.13%, respectively. This study provides theoretical and experimental evidence for the establishment of the theoretical model of the stagnant region in mechanical scratching, the analysis of its forming mechanism, and the control of the stagnant region geometric parameters on the formed groove surface.

Keywords Stagnant region, Mechanical scratching, Negative rake angle tool, Adhesive internal friction, Groove surface quality

Mechanical scratching technology can realize green, low-cost, large-area, and high-precision machining, thus it is widely used in microstructure machining. The processing quality of microstructure directly determines its performance, thus how to produce high-quality microstructure has become an urgent problem in manufacturing science. When the scratching-diamond wedge tool (scratching tool) mechanically scratches the plastic metal material, the formed groove surface will produce a plastic flow region and a stagnant region with obvious

¹College of Mechanical and Electric Engineering of Jilin Institute of Chemical Technology, Jilin 132022, China. ²College of Mechanical and Electric Engineering of Changchun University of Science and Technology, Changchun 130022, China. ✉email: dycust@126.com; sgfcust@126.com

boundaries^{1,2}. The stagnant region will affect the groove quality and tool wear. Therefore, solving the stagnation problem of the mechanical scratching material has become the key to improving the groove quality. However, there is little research on the stagnant region in mechanical scratching, so it is of great significance to study the forming mechanism and evolutionary pattern of the stagnant region in mechanical scratching to perfect the mechanical scratching forming theory and improve the formed groove quality.

Currently, the theoretical and experimental research on the material stagnation phenomenon in metal cutting is predominantly conducted through orthogonal cutting. The occurrence of this phenomenon in metal cutting machining affects the material flow characteristic, which in turn influences the quality of the machined surface. Consequently, scholars have conducted exploratory research into the stagnant phenomenon. Ohbuchi and Obikawa³ have indicated that a stagnant region forms on the tool surface, which replaces the tool's cutting and plowing actions on the material, and the stagnant point diverts the material during orthogonal cutting with a negative rake angle tool. Ozturk et al.⁴ have also noted that, in the study of stagnant points in micro-cutting, it is the stagnant region rather than the stagnant point that affects material flow. This means that, in the orthogonal cutting process with a negative rake angle tool, the stagnant region, not the stagnant point, is what influences material flow. Scholars have developed cutting models that take into account the stagnant region based on its influence on material flow. Abebe⁵ proposed the first cutting model to consider the stagnant region of a negative rake angle tool. Building on the second cutting model of Lee and Shaffer⁶, Fang⁷ established a slip-line field cutting model for a large negative rake angle tool, which includes three deformation regions, with the stagnant region being one of them. It has been concluded that the boundary length of the stagnant region is related to the friction coefficient at the contact interface. Ozturk et al.⁸ developed a slip-line field cutting model for a negative rake angle tool that considers the stagnant region, using the matrix technique of Dewhurst and Collins. They studied the influence of the negative rake angle on the area of the stagnant region, the cutting force, and the chip thickness as the negative rake angle changed from 0° to -70°. The results showed that the larger the absolute value of the negative rake angle, the larger the area of the stagnant region. Ozturk et al.⁹ also established a slip-line field cutting model for a round-edge tool that considers the stagnant region and verified the model based on the material plastic deformation mechanism in micro-cutting CuZn30 with a round-edge tool. Zhang et al.¹⁰ proposed a slip-line field cutting model for a negative chamfer tool that considers the stagnant region. This model also includes three main deformation regions, and the stagnant region in front of the negative chamfer influences material flow. Uysal¹¹ developed a slip-line field cutting model for a worn tool that considers the stagnant region and solved for parameters such as the size of the tool wear region and the stagnant region, the chip curl radius, the chip thickness, and the first shear slip field, according to experimental cutting force data.

To investigate the formation mechanism and evolution of the stagnant region more deeply, scholars have conducted experimental studies from various perspectives. Kita¹² found that a larger stagnant region forms in front of the tool surface during orthogonal cutting with a pyramid-shaped cutting tool, while a higher material removal rate is achieved with a conical cutting tool. Ohbuchi and Obikawa⁵ noted that a larger stagnant region forms during orthogonal cutting with a large negative rake angle tool compared to conical and pyramidal cutting tools, and the thickness of the stagnant region increases as the absolute value of the rake angle increases. Wan Lei¹³ investigated the influence of tooltip shapes (sharp corner, round corner, negative chamfer, and double negative chamfer) on the stagnant region area through orthogonal cutting experiments on AlSi1045. The results showed that the largest stagnant region area forms in front of the negative chamfer tool. Kita et al.¹² found that the higher the cutting speed, the lower the height of the stagnant point formed when cutting carbon steel with a negative rake angle tool. Weule et al.¹⁴ also pointed out that a lower cutting speed is an important factor in the occurrence of the stagnation phenomenon. Usui and Makino¹⁵ indicated that a large stagnant region forms in front of the tool surface during low-speed cutting with a large negative rake angle tool, and the formation of the stagnant region may be related to the mechanical properties of the cutting material. Kountanya and Endres¹⁶ found that a more pronounced and larger stagnant region forms in front of a blunt tool surface when cutting brass orthogonally, whereas a smaller stagnant layer forms when cutting pure zinc, showing that the mechanical properties of the cutting material affect the formation of the stagnant region. Using orthogonal cutting experiments on AlSi1045 with a negative chamfer tool, Wan et al.¹⁷ studied the effect of the tool-chip boundary friction coefficient on the stagnation phenomenon. The results showed that the larger the friction coefficient, the more likely the material stagnation phenomenon will occur in front of the tool surface, and the larger the stagnant region will be.

Scholars have also studied the effects of the stagnation phenomenon that occurs during cutting with negative rake angle tools. In the study of orthogonal cutting alloy steel with a negative rake angle tool, Komanduri¹⁸ noted that the stagnant region affects material flow diversion, with some material bypassing the stagnant region and flowing upward along the tool surface to form a chip, while other material bypasses the region and flows downward to create the machined surface. Ozturk et al.¹⁹ found through orthogonal cutting of CuZn30 with a negative rake angle tool that the greater the absolute value of the tool's negative rake angle, the higher the ratio of normal force to tangential force, and the larger the areas of plastic deformation and stagnation on the tool surface, resulting in a better quality machined surface. Anilcandra and Surappa²⁰ also observed that the quality of the machined surface is superior with a -15° rake angle tool compared to a -5° rake angle tool in orthogonal cutting of pure magnesium. Hoshi²¹ indicated that a stagnant region forms in front of the negative chamfer when the contact length between the tool and the chip exceeds the length of the negative chamfer, which protects the tool and extends its service life. Agmell et al.²² examined the wear mechanism of the CNMG120408 MF4 TP2500 tool through orthogonal cutting AISI4140 experiments with both rounded edge and negative chamfer tools. They found that the stagnant region in front of the negative chamfer tool is larger and protects the tool surface because the material in the stagnant region is stationary. Additionally, due to the restriction of the negative chamfer on material flow, most of the stagnation material flows into the machined surface, increasing the depth of the hardened layer. Guo et al.²³ discovered that the stagnation material determines the minimum cutting depth, which

in turn affects the surface residual stress, and when the cutting depth reaches the minimum cutting thickness, it produces a unique hook profile in the surface residual stress.

In summary, the geometric characteristics of the cutting tool are an important external factor in the formation of the stagnant region; changes in cutting speed, material properties, and boundary friction conditions can also affect the generation and evolution of the stagnant region. Additionally, the formation of the stagnant region influences material flow characteristics, the quality of the machined surface, and tool wear. Although scholars have studied the theories and experiments of stagnant region related to the negative rake angle tool, round-edge tool, negative chamfer tool, worn tool in orthogonal cutting, there is still no unified explanation for the formation mechanism of the stagnant region. Furthermore, there are no reports on the formation mechanism and influence of the stagnant region in mechanical scratching. Therefore, this paper will use a scratching-diamond wedge tool to mechanically scratch plastic metal materials as a basis for studying the formation mechanism and evolutionary pattern of the stagnant region, and the main research contents are as follows. Firstly, a theoretical model will be established to calculate the geometric parameters of the stagnant region on the formed groove surface, based on the friction partition mechanism and slip-line field theory. Secondly, the formation process and characteristics of the stagnant region will be analyzed through simulation and experimentation. Thirdly, the characteristics of the stagnant region will be analyzed through simulation and experimentation. Finally, the evolutionary regularity of the stagnant region under the influence of mechanical scratching parameters will be investigated using scratching experiments and the theoretical model.

Theoretical calculation model of geometric parameters of the stagnant region on the formed groove surface

As shown in Fig. 1a, the scratching tool will be used for mechanically scratching the metal materials in this article. During mechanical scratching, the main edge is directed forward, namely the direction of the main edge is aligned with the scratching direction. The scratching tool is raised at a certain elevation angle. Then, the main edge blade splits the metal material or coating, and the two negative rake angle contact surfaces act on the material with cutting and extrusion. The deformed material is extruded into the groove by the two deputy edges. As shown in Fig. 1b, the formed groove will be created by repeatedly cycling this mechanical scratching process as the workpiece moves along the index positioning direction.

Working negative rake angle of the scratching tool

As seen from the geometric model of the working negative rake angle of the scratching tool in Fig. 2, the X, Y, and Z axes represent the index positioning direction, the mechanical scratching direction, and the mechanical

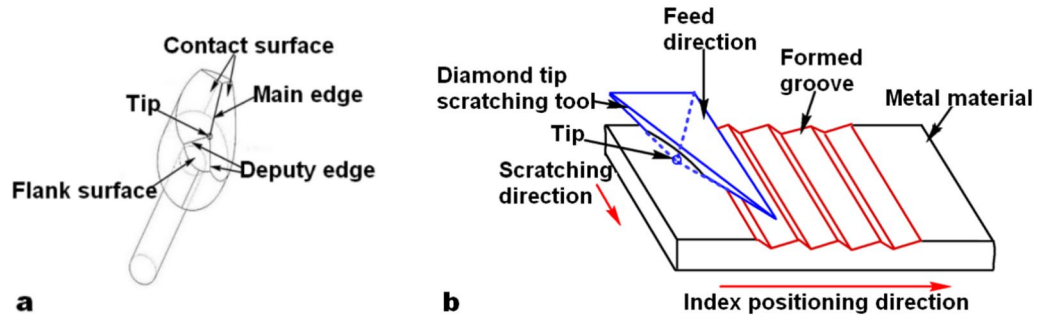


Figure 1. Schematic diagram of mechanical scratching (a) diamond wedge scratching tool (b) formed groove.

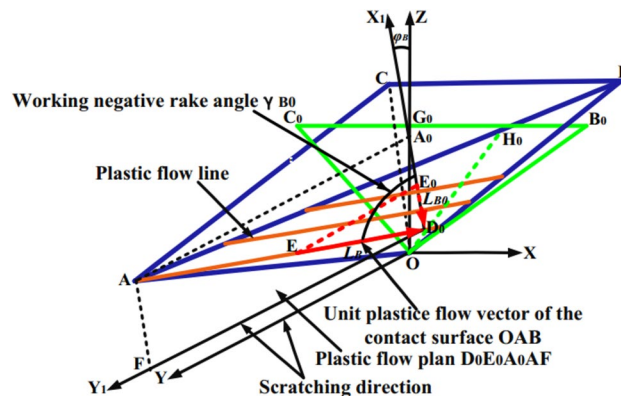


Figure 2. Geometry model of working negative rake angle of the scratching tool.

scratching depth direction, respectively. The multi-cutting tool cutting theory²⁴ indicates that oblique cutting and mechanical scratching of plastic metal materials with the scratching tool²⁵ can be likened to the cutting and extrusion forming effects of a negative rake angle tool on the material in the plastic flow plane. Utilizing the theoretical model of the unit plastic flow vector of the contact surface¹, the working negative rake angle of the scratching tool can be determined in the plastic flow plane. By definition, the negative rake angle is the complementary angle to the angle between the unit plastic flow vector and the scratching direction vector in the plastic flow plane $D_0E_0A_0AF$, as depicted in Fig. 2. Consequently, the absolute values γ_{B0} and γ_{C0} of the working negative rake angle for the contact surfaces OAB and OAC can be expressed as follows:

$$\gamma_{B0} = \frac{\pi}{2} - \arccos \left(\frac{\vec{L}_B \cdot \vec{y}}{|\vec{L}_B| \cdot |\vec{y}|} \right) = \frac{\pi}{2} - \arccos \left(\frac{-n_{Bx}m_B \sin \varphi_B + n_{Bz}m_B \cos \varphi_B}{n_{By}} \right) \quad (1)$$

$$\gamma_{C0} = \frac{\pi}{2} - \arccos \left(\frac{\vec{L}_C \cdot \vec{y}}{|\vec{L}_C| \cdot |\vec{y}|} \right) = \frac{\pi}{2} - \arccos \left(\frac{n_{Cx}m_C \sin \varphi_C + n_{Cz}m_C \cos \varphi_C}{n_{Cy}} \right) \quad (2)$$

where

$$m_B = \sqrt{\frac{1}{1 + \left(\frac{n_{Bx} \sin \varphi_B - n_{Bz} \cos \varphi_B}{n_{By}} \right)^2}}$$

$$m_C = \sqrt{\frac{1}{1 + \left(\frac{n_{Cx} \sin \varphi_C - n_{Cz} \cos \varphi_C}{n_{Cy}} \right)^2}}$$

φ_B (φ_C) is the angle between the projection of the unit plastic flow vector \vec{L}_B (\vec{L}_C) and the normal axis Z in the base plane XOZ. L_B and L_C are the unit plastic flow vectors of the contact surface OAB and OAC, respectively. \vec{y} is the unit vectors along the Y axes. n_{Bx} , n_{By} , n_{Bz} and n_{Cx} , n_{Cy} , n_{Cz} are the coordinate values of the unit normal vector \vec{n}_B and \vec{n}_C of the contact surface OAB and OAC, respectively.

Geometric parameters of the stagnant region in the plastic flow plane

According to research on the plastic flow characteristics of materials in mechanical scratching, it can be concluded that, given engraving processing parameters, the plastic flow direction of the material on the tool surface and the working negative rake angle of the scratching tool will be determined. When the tool's rake angle is fixed, the stress and deformation characteristics of characteristic points in the plastic flow plane can be studied through metal cutting theory. Currently, the main methods for studying metal plastic deformation theory include the elementary analytical method, slip line method, upper bound method, and variational method^{26,27}. The slip line method is primarily used to solve the plane strain problem of plastic materials. Compared to other plastic deformation theories and methods, the slip line method can clearly express the material's plastic flow situation within the shear deformation region and calculate important parameters such as the size of the deformation zone and cutting force. Therefore, based on Lee and Shaffer's second cutting slip line field model²⁸, this article establishes a negative rake angle tool cutting slip line field model in the plastic flow plane AD_0I that considers the friction partition mechanism and stagnation phenomenon, as shown in Fig. 3a. This slip-line field model consists of four regions, and the physical meanings and stress states of each region are explained as follows:

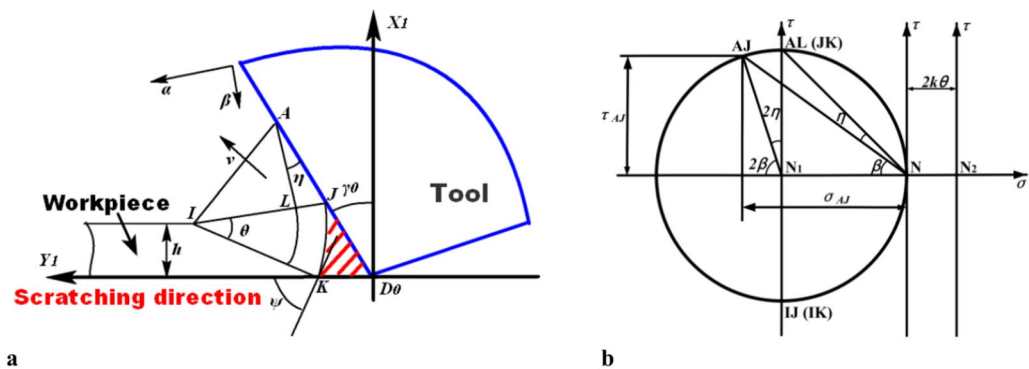


Figure 3. Theoretical Model of negative rake angle tool in mechanical scratching (a) slip line field model (b) stress Mohr's circle.

Triangular region AIJ: Simplify plastic deformation of chip or material into a triangular region AIJ with uniform stress distribution, where IJ represents the maximum shear stress in the same direction as the slip line α (the other slip-line β is in the same direction as AL and perpendicular to IJ). An angle of 45° between AI and IJ represents the main plane direction of the plastic deformation region, which is also the upper boundary of the plastic deformation region. AJ corresponds to the external friction contact region between the tool-material. The stress state of each point on the triangular region AIJ can be represented by the stress Mohr's circle as shown in Fig. 3b, where NN_1 is equal to the average hydrostatic pressure in the uniform stress field.

Fan-shaped IJK: The region starts from IJ , turns around point I through slip-line angle θ , and forms a fan-shaped deformation region IJK connected to the stagnant region. The region represents the first deformation region where the material undergoes shear-slip deformation. The stress state at each point on the sector IJK can be represented by a straight line passing through point N_2 and parallel to the τ axis, where NN_2 is equal to $2k\theta$.

Triangular region ALJ: The slip-line angle η is determined by the friction conditions of the tool-material. According to the friction partition mechanism of the tool-material, AJ corresponds to the outside friction contact region of the tool-material. Under extreme conditions, the frictional shear stress of the contact interface is equal to the shear flow stress k , and the triangular region ALJ will disappear.

Red shaded region JD_0K : ψ is the top angle. According to the friction partition mechanism of the tool-material, JD_0 corresponds to the outside friction contact region of the tool-material, JD_0K is the stagnant region, where the boundary point J of the internal and external friction partition is the top point of the stagnant region.

According to the three-way force balance relationship of mechanical scratching¹, the average normal stress p and the average friction coefficient μ on the contact surface of the tool-material can be calculated. Based on the slip-line field model, the slip-line angle η corresponding to the plastic flow region AJL can be calculated represented as:

$$\eta = \frac{\pi}{4} - \frac{\arctan(\mu)}{2} \quad (3)$$

Simultaneously, the slip-line angle θ corresponding to the fan-shaped region IJK can be obtained as:

$$\theta = \frac{1}{2} \left(\frac{P_I}{k} - 1 \right) \quad (4)$$

where P_I/k is the hydrostatic pressure of point I (dimensionless).

Due to the average normal stress P on the contact surface of the tool-material being equal to σ_{AJ} , then P_I can be expressed as:

$$P_I = \sigma_{AJ} - \tau_{AJ} \sin(2\eta) = \sigma_{AJ} - \sigma_{AJ}\mu \sin(2\eta) \quad (5)$$

Then Eq. 4 can be transformed into:

$$\theta = \frac{1}{2} \left(\frac{\sigma_{AJ} - \sigma_{AJ}\mu \sin(2\eta)}{k} - 1 \right) \quad (6)$$

According to the slip-line field, the top angle ψ of the stagnant region JKD_0 can be determined as:

$$\psi = \frac{\pi}{4} + \frac{\arctan(\mu_{av})}{2} + \gamma_0 - \theta \quad (7)$$

where μ_{av} is the adhesive friction coefficient corresponding to the external friction contact region (stagnant region) between the tool-material. According to the modified adhesion theory, the adhesive friction is determined by the material's shear flow stress k . γ_0 is the absolute value of the negative rake angle of the scratching tool.

Based on the slip-line field and the above angle parameters, the geometric parameters KD_0 and JD_0 of the stagnant region JKD_0 in the plastic flow plane can be obtained as:

$$KD_0 = \frac{h(\cos(\eta) - \cos(\eta + \theta))}{\cos(\psi) \cos(\gamma_0)} \quad (8)$$

$$JD_0 = \frac{h(\cos(\eta) - \cos(\eta + \theta)) \cos(\eta + \frac{\theta}{2} - \gamma_0)}{\cos(\psi) \cos(\gamma_0) \sin(\eta + \frac{\theta}{2})} \quad (9)$$

where h is the depth of scratching.

Geometric parameters of the stagnant region on the formed groove surface

As shown in Fig. 3a, it can be seen that KD_0 represents the extension length of the stagnant region towards into the material in the plastic flow plane, JD_0 represents the stagnant region length in the plastic flow plane, and the stagnant region length along the plastic flow direction on the formed groove surface. JD_0 can be indirectly measured through experiments, while KD_0 cannot be directly measured through experiments. Therefore, JD_0 will be used as the basic comparison parameter to investigate the influence of scratching processing parameters on the stagnant region in this article, and JD_0 will be represented by lp -sg. To facilitate experimental measurement and analysis, the following three stagnant region geometric parameters are introduced based on lp -sg, based on the space vector relationship (refer to Fig. 2, taking the front surface OAB as an example):

As shown in Fig. 4a, the stagnant region length on the formed groove surface l_{B-sg} is equal to the projection of stagnant region length in plastic flow plane l_{p-sg} on the XOY base plane, then l_{B-sg} can be expressed as:

$$l_{V-sg} = \frac{\sin(\gamma_{0B}) \sin(\varphi_{Bxy})}{\cos\left(\arctan\left(\frac{x_B}{z_B}\right)\right)} \frac{h(\cos(\eta) - \cos(\eta + \theta))\left(\eta + \frac{\theta}{2} - \gamma_{0B}\right)}{\cos(\psi) \cos(\gamma_{0B}) \sin\left(\eta + \frac{\theta}{2}\right)} = M_1 l_{p-sg} \quad (10)$$

where γ_{0B} is the absolute value of the tool working negative rake angle. φ_{Bxy} is the projection angle of the unit plastic flow vector corresponding to the material plastic flow line, which is called the plastic flow direction angle. (x_B, y_B, z_B) is the coordinate value of the contact vertex B of the tool-material¹.

As shown in Fig. 4b, the stagnant region length on the formed groove surface in top view l_{V-sg} represents the projection of the stagnant region length on the formed groove surface l_{B-sg} on the XOY base plane. Which is mainly used for comparative analysis with the experimental value of the stagnant region length on the formed groove surface in the top view. Then l_{V-sg} can be expressed as:

$$l_{V-sg} = \sin(\gamma_{0B}) \sin(\varphi_{Bxy}) \frac{h(\cos(\eta) - \cos(\eta + \theta))\left(\eta + \frac{\theta}{2} - \gamma_{0B}\right)}{\cos(\psi) \cos(\gamma_{0B}) \sin\left(\eta + \frac{\theta}{2}\right)} = M_2 l_{p-sg} \quad (11)$$

Then, the ratio Δl_{sg} of the stagnant region length on the formed groove surface in the top view l_{V-sg} to the one side length of the formed groove in the top view l_V can be further expressed as:

$$\Delta l_{sg} = \frac{l_{V-sg}}{l_V} = \frac{\sin(\gamma_{0B}) \sin(\varphi_{Bxy})}{h_B a \tan\left(\frac{x_B}{z_B}\right)} \frac{h(\cos(\eta) - \cos(\eta + \theta))\left(\eta + \frac{\theta}{2} - \gamma_{0B}\right)}{\cos(\psi) \cos(\gamma_{0B}) \sin\left(\eta + \frac{\theta}{2}\right)} = M_3 l_{p-sg} \quad (12)$$

The above expressions indicate that the stagnant region's geometric parameters l_{B-sg} , l_{V-sg} , and Δl_{sg} are determined by the stagnant region length in plastic flow plane- l_{p-sg} and the conversion parameters M_1 , M_2 , and M_3 . From expression (9), it can be seen that l_{p-sg} is related to the scratching depth, scratching tool's working negative rake angle, hydrostatic pressure P_f/k at point I in the plastic flow plane, and friction coefficient. M_1 is determined by the unit plastic flow vector and formed groove's geometric parameters. M_2 is determined by the unit plastic flow vector. M_3 is determined by the unit plastic flow vector, formed groove's geometric parameters, and the lateral ridge height. Therefore, the changing rules of the stagnant region's geometric parameters on the formed groove surface are extremely complex, and controlling the boundary of the stagnant region will become more

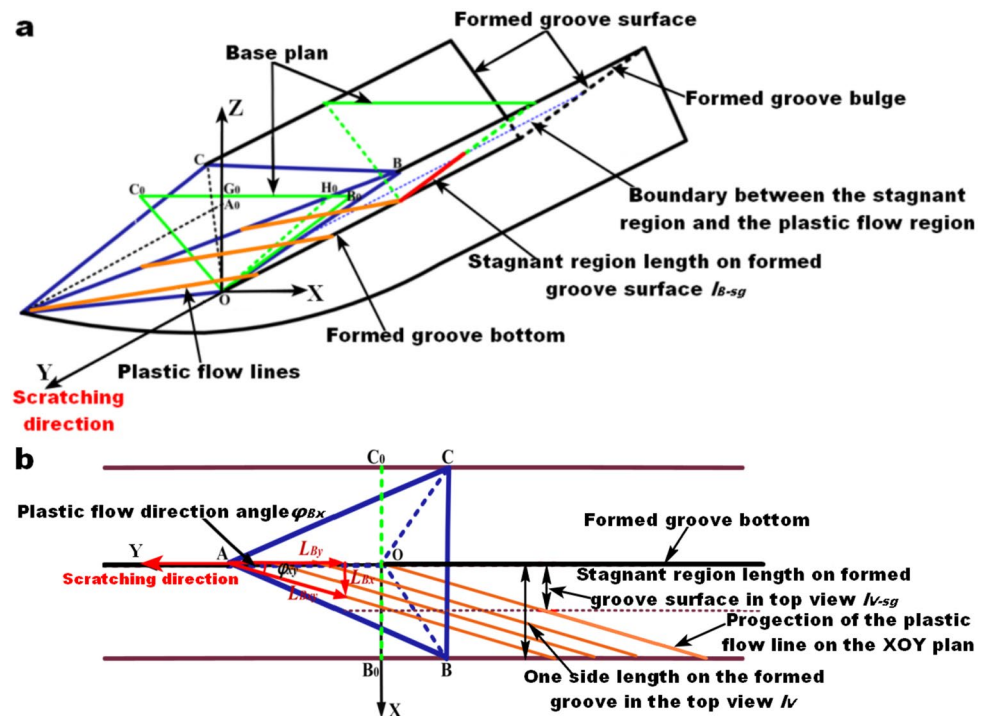


Figure 4. Geometric parameters of the stagnant region on the formed groove surface (a) stagnant region length on the formed groove surface l_{B-sg} (b) stagnant region length on the formed groove surface in top view l_{V-sg} and the ratio Δl_{sg} of the stagnant region length on the formed groove surface in top view l_{V-sg} to the one side length of the formed groove in top view l_V .

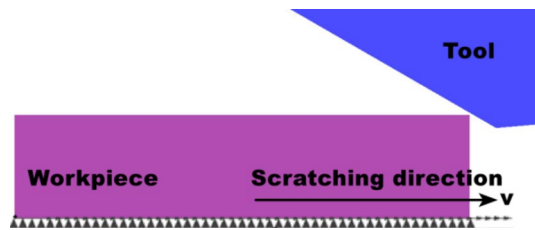


Figure 5. 2D-FEM of the orthogonal cutting of the negative rake angle tool.

difficult. The establishment of this theoretical model will lay a theoretical foundation for studying the influence of machining scratching processing parameters on the stagnant region boundary.

Ethical approval

The authors claim that they are non-life science journals and there are no ethical issues.

Consent to participate

The authors claim that they agree to participate.

Mechanical scratching finite element simulation and experiment

In order to study the forming mechanism and evolutionary pattern of the stagnant region in mechanical scratching, this paper first investigates the formation process of the stagnant region in the plastic flow plane using finite element simulation. Then analyzes the characteristics of the stagnant region on the formed groove surface through mechanical scratching experiments. Final analysis of the evolutionary pattern of the stagnant region under the influence of the mechanical scratching parameters using scratching experiments and the theoretical model.

Simulation model of cutting tool with negative rake angle in plastic flow plane

It is difficult to show the instantaneous deformation inside the material in mechanical scratching using experiments. Therefore, the orthogonal cutting simulation of the negative rake angle tool in the plastic flow plane will be used to investigate the formation process of the stagnant region in mechanical scratching^{29,30}. The FEM of the orthogonal cutting simulation in the plastic flow plan is implemented by DEFORM molding software. The 2D-FEM of the orthogonal cutting with the negative rake angle tool is shown in Fig. 5. The basic parameters of the orthogonal cutting model are as follows: the simulation was carried out with a 1:1 scale for both the workpiece and the cutting tool, the tool is fixed and the workpiece moves at uniform speed, the cutting speed is 1 mm/s, the cutting depth is 200 μm . The simulation analysis form is deformation and heat exchange, the analysis step is 5000, and the analysis step interval is 0.03 s. The cutting tool adopts a scratching-diamond wedge tool. The negative rake angle of the tool is -60° , the relief angle of the tool is 5° , assuming the edge radius of the tool is sharp ($R=0^\circ$), the tool is modeled as a rigid material, the material properties of the tool is $E=1140\text{GPa}$ Poisson's ratio = 0.07. Copper-T2 is used for the scratching materials in this experiment. It is assumed to be isotropic with no residual stress. The workpiece is made of T2 material, with dimensions of 6 mm x 1.6 mm, and the number of mesh divisions is 300,000. The material properties of T2 is $E=115\text{GPa}$ Poisson's ratio = 0.34, The Johnson–Cook (J–C) material model³¹ is used to describe the true stress–strain relationship of the material as the following equation:

$$\sigma = (A + B\varepsilon^n) \left(1 + C \ln \frac{\dot{\varepsilon}}{\dot{\varepsilon}_0} \right) \left(1 + \left(\frac{T - T_r}{T_m - T_r} \right)^m \right) \quad (13)$$

where σ , ε , $\dot{\varepsilon}$, $\dot{\varepsilon}_0$ are the equivalent flow stress, equivalent plastic strain, equivalent plastic strain rate, and reference strain rate, respectively. T_m and T_r are the material melting temperature and reference ambient temperature, respectively. The J–C constitutive plasticity model parameter of T2 is shown in Table 1.

Mechanical scratching experiment

Experimental setup

To investigate the characteristics of the stagnant region on the formed groove surface and further analyze the evolutionary pattern of the stagnant region under the influence of mechanical scratching parameters, mechanical scratching experiments were conducted. As shown in Fig. 6a, an ultra-precision, vertical, computerized numerical control (CNC) scratching machine (GP100) was employed for the experiments. Laser diffraction was used

| Material | A(MPa) | B(MPa) | n | C | m |
|----------|--------|--------|------|-------|------|
| T2 | 123.7 | 435.1 | 0.31 | 0.022 | 0.83 |

Table 1. Material parameter values for the J–C model of T2.

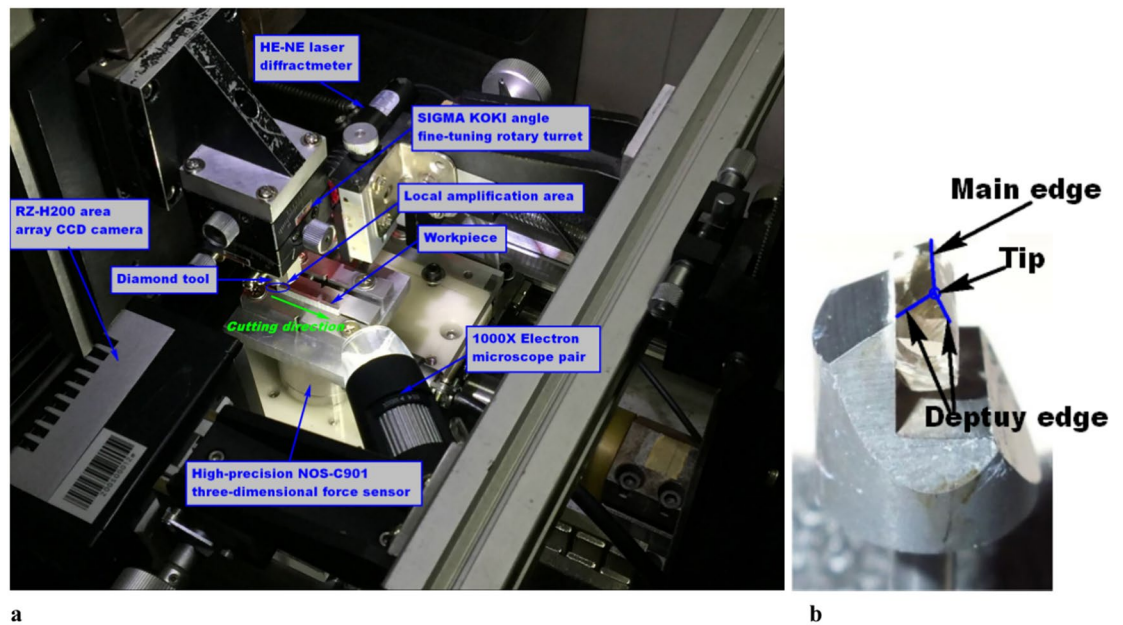


Figure 6. Experimental setup (a) scratching machine—GP100 (b) diamond wedge scratching tool.

| Mechanical scratching parameters | Experimental value |
|---|----------------------|
| Scratching tool geometry parameters | |
| Wedge angle θ_w (°) | 80, 85, 90 |
| Relief angle θ_B (°) | 30, 35, 40 |
| Scratching tool installation parameters | |
| Rotation angle around X axis (°) | -5, -2.5, 0, 2.5, 5 |
| Rotation angle around Y axis (°) | -5, -2.5, 0, 2.5, 5 |
| Rotation angle around Z axis (°) | -5, -2.5, 0, 2.5, 5 |
| Scratching speed (mm/s) | 0.1, 1, 10, 100, 500 |
| Scratching material | T2, Al1060 |
| Scratching depth (μm) | 200 |

Table 2. Mechanical scratching condition.

to achieve accurate tool setting with an HE–NE laser diffractometer and an RZ-H200 area array CCD camera³². The scratching force was measured and recorded online during the scratching process using a high-precision NOS-C901 three-dimensional force sensor. A SIGMA KOKI angle fine-tuning rotary turret, made in Japan, was used to clamp and rotate tools, with the tool rotation angle deviation controlled at $\pm 5^\circ$ to ensure accuracy. A diamond wedge scratching tool was used in the scratching experiments (Fig. 6b). The geometric parameters of the scratching tool¹ are as follows: wedge angle of 85° , B side angle of 47.5° , relief angle of 35° , edge radius of 215.6 nm, and the length of the main edge of 2.65 mm.

Mechanical scratching condition

According to the theoretical calculation model of the geometric parameters of the stagnant region on the formed groove surface, the main factors affecting the geometric parameters of the stagnant region on the formed groove surface are the scratching tool's negative rake angle, the hydrostatic pressure $P_{I/k}$ at the I point in the plastic flow plane, the friction coefficient, the unit plastic flow vector, and the geometric parameters of the formed groove. Therefore, the geometric parameters of the scratching tool (wedge angle θ_w , relief angle θ_B), installation parameters of the scratching tool (rotation angle of the scratching tool around three coordinate axes, counterclockwise rotation angle is positive), scratching speed and material will be used as the scratching experiment parameters. In order to facilitate the stagnant region boundary on the formed groove surface and reduce the influence of the mechanical scratching error on the geometric parameters of the stagnant region on the formed groove, a large scratching depth will be used in the scratching experiment, and the marking depth is 200 μm . The mechanical scratching parameters are shown in Table 2.

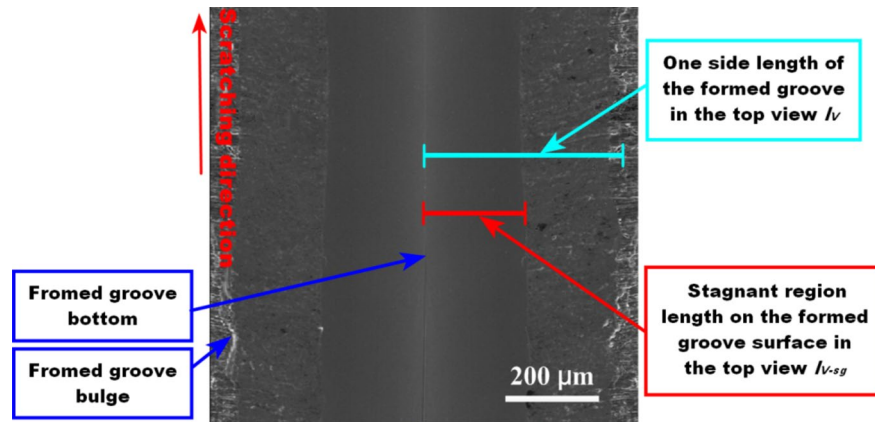


Figure 7. Experimental measurement of the geometric parameters of stagnant region on the formed groove surface.

Measurement of the experimental values of stagnant region geometric parameters

The geometric parameters of the stagnant region on the formed groove surface were measured using a scanning electron microscope (SEM). As shown in Fig. 7, a clear demarcation phenomenon is visible on the formed groove surface^{33,34}. The length of the dense tissue region from the bottom of the formed groove to approximately the middle of the groove characterizes the stagnant region length in the top view l_{v-sg} , which corresponds to the side length of the formed groove in the top view l_v . l_{v-sg} and l_v will be used as the experimental test objects for comparing the theoretical and experimental values of the geometric parameters of stagnant region on the formed groove surface under the influence of mechanical scratching parameters. To ensure the reliability of the experimental values, the experimental values of l_{v-sg} and l_v were measured at 50 equally spaced locations along the scratching direction on the corresponding side-formed groove surfaces under the specific mechanical scratching condition, and the average values were taken as the final experimental values, respectively.

Results and discussion

Analysis of the forming process of the stagnant region in the plastic flow plane

Based on the 3.1 simulation model of the cutting tool with a negative rake angle in the plastic flow plane, simulation results were obtained for a -60° negative rake angle scratching tool. The FEM simulation distributions of stress, strain, velocity, and temperature were extracted, as shown in Fig. 8. From Fig. 8a–c, it can be observed that due to the cutting and squeezing effects of the tool's negative front surface on the material, a band-shaped stress concentration region is formed between the tooltip and the free contact surface of the material. The material undergoes shear-slip deformation in this region, which is the first deformation region. After flowing through the first deformation region, the material will undergo secondary plastic flow along the leading edge of the stagnant region and the tool surface, resulting in the formation of chips or plastic bulges until it terminates at the tool-material separation point. This region is the external friction region, or the second deformation region. Due to the stretching and squeezing effects of the tooltip and back face on the formed surface, the contact area between the tooltip and the formed surface will form the highest strain deformation region, which is the third deformation region. Due to the geometrical characteristics of the tool's negative front surface, the material outflow along the front face is constrained. Moreover, due to the excessive squeezing effect of the tool's negative front surface on the material, the material yields under force, forming an adhesive internal friction region inside the material. Consequently, a material stagnant region with minimal strain and velocity, approximately triangular in shape, is formed near the tooltip. From the velocity distribution cloud in Fig. 8c, it can be observed that the stagnant region has a diversion effect on the material, altering the working negative rake angle of the tool. According to the temperature distribution cloud in Fig. 8d, the highest temperature is 20.4°C , indicating that temperature has little effect on material deformation during medium and low-speed mechanical scratching.

In order to present the formation process of the stagnant region in the plastic flow plane clearly, the stress distribution cloud of different analysis steps is extracted as shown in Fig. 9. Comparison can be seen that when the analysis step 200, the tool contacted with the material, due to the negative front surface geometry characteristics of the excessive extrusion effect on the material, an adhesive internal friction effect is formed inside the material, and the plastic flow of the material is restricted, therefore a less stressful plastic deformation stagnant layer formed in the tool's front surface. When the tool continues to move forward, the analysis step increases from 210 to 300, the material internal adhesion friction intensifies, and the stagnant layer of the tool's front surface is superimposed layer by layer to form a triangular stagnant region. The growth process of the stagnant region is as follows: at the beginning, due to the dramatic increase of adhesive friction within the material, the stagnant region grows rapidly. When the stagnant region grows large enough, the adhesive friction within the material reaches a peak and begins to decay. Meanwhile, the growth rate of the stagnant region begins to decrease. When the analysis step continues increased from 320 to 340, the adhesive friction within the material of the stagnant region basically disappears, and then the effective geometric characteristics of the tool's negative front surface cannot continue to restrict the material outflow and deformation (the tool's actual working negative rake angle

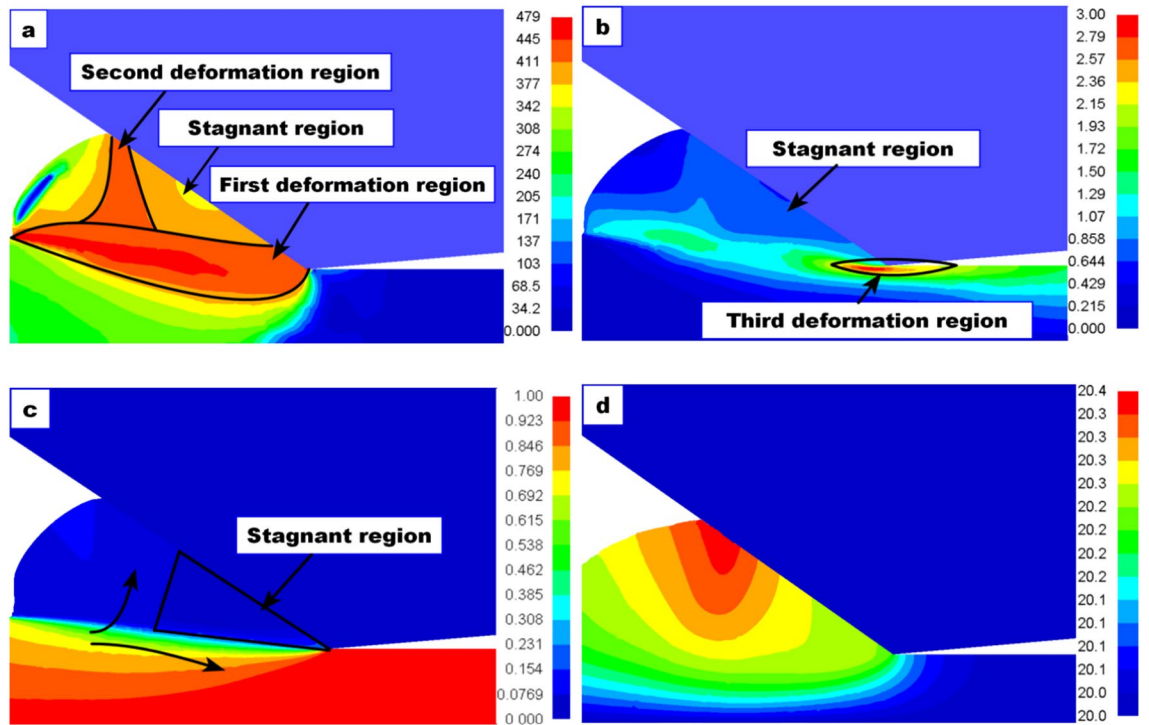


Figure 8. FEM simulation distribution cloud (a) stress distribution cloud (b) strain distribution cloud (c) velocity distribution cloud and (d) temperature distribution cloud.

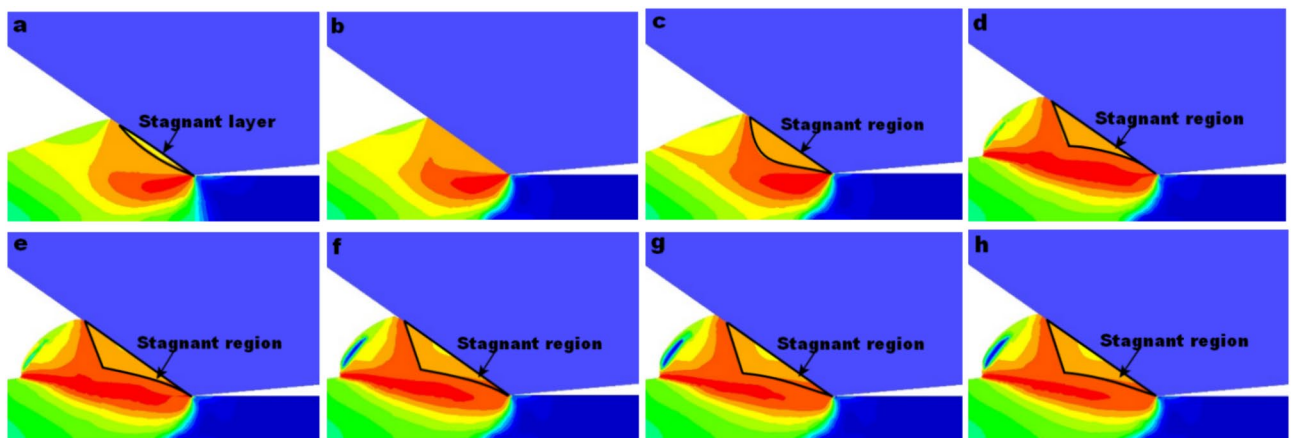


Figure 9. Stress distribution cloud of different analysis steps (a) step 200 (b) step 210 (c) step 220 (d) step 230 (e) step 240 (f) step 300 (g) step 320 and (h) step 340.

changes due to the stagnant region area). During the process, the front edge of the stagnant region no longer grows, and the shape of the stagnant region remains unchanged.

In summary, during low and medium-speed mechanical scratching, the temperature of the plastic deformation material in the plastic flow plane is close to room temperature. Therefore, the stagnant region is not a product of forming processes such as cold welding or pressure fusion, but a plastic deformation region formed due to the geometrical characteristics of the negative front surface of the scratching tool and its excessive extrusion acting on the material, leading to the formation of an adhesive friction within the material. The above simulation and analysis results elucidate the mechanism of adhesive internal friction molding in the stagnant region.

Analysis of the characteristics of the stagnant region

Based on 3.2 mechanical scratching experiments, it can be observed that after scratching plastic metal materials with a scratching-diamond wedge tool, the formed groove surface will exhibit a stagnant region and a plastic flow region, with an obvious boundary phenomenon between the two regions. Consequently, these two regions will inevitably have a different impact on the quality of the formed groove surface. This paper will analyze the

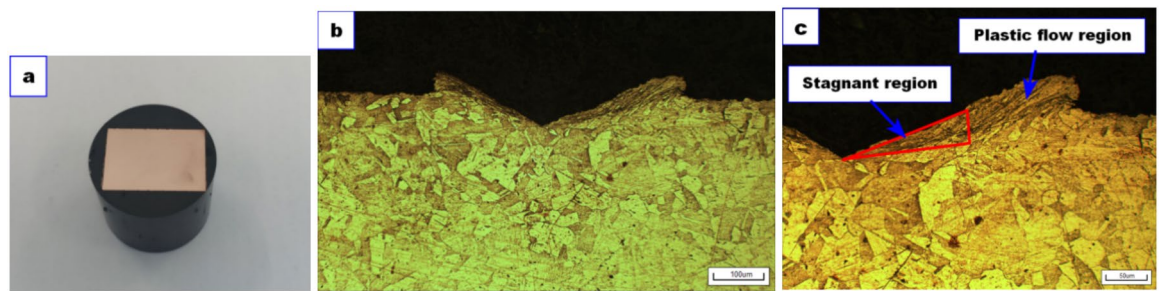


Figure 10. Cross-section of the formed groove: (a) inlay sample of the formed groove cross-section (b) the metallographic organization of the formed groove cross-section and (c) the partial enlargement of the metallographic organization of the formed groove cross-section.

characteristics of the stagnant region by examining the effects of the two regions on the metallographic microstructure, surface hardness, and surface roughness of the formed groove surface.

Metallographic microstructure analysis

Based on 3.2 mechanical scratching experiments, the more easily corroded T2 material was selected for scratching experiments. The formed groove was taken for wire cutting and inlaying of its cross-section. After grinding, polishing and FeCl₃ etching treatment, the metallographic organization of the formed groove cross-section was observed and extracted by using PTI MPC-400 optical microscope as shown in Fig. 10a,b.

From the partial enlargement of the metallographic organization of the formed groove cross-section in Fig. 10c. It can be seen the crystal particle arrangement in the formed groove can be divided into three regions. The first is in the area of the T2 base material away from the groove surface, the crystal particle distribution is relatively uniform, and obvious boundaries of the crystal particle are visible. The second is in the region of an approximate triangle at the groove bottom, the crystal particle size is small, and the crystal particle of the out edges of the triangle region show a small stretching, and the stretching direction is approximately parallel to the groove surface. The third is near the bulge region of the groove, the crystal particle appears to be substantial stretching and fibrous, and the stretching direction is approximately parallel to the groove surface. From the above crystal particle arrangement of the formed groove cross-section and the 4.1 the forming process of the stagnant region in the plastic flow plane, it can be seen that the approximate triangle region of the groove bottom is the stagnant region, the region near the bulge region of the groove is the plastic flow region. The analysis of the crystal particle arrangement and size of the formed groove cross-section shows that the stagnant region is dominated by extrusion deformation, and the plastic flow region is dominated by substantial stretching deformation.

Based on 3.2 mechanical scratching experiments, scratching experiments were performed on T2 and Al1060 materials, respectively. EVO MA 25/LS scanning electron microscope was used to observe and extract the microstructure of the unilateral groove surface in the top view of the two materials after scratching as shown in Fig. 11. From Fig. 11a,b, it can be seen that the corresponding formed groove surface of two materials shows obvious partitioning phenomena. In order to observe the microstructure of the materials near the boundary line clearly, the region near the boundary line is locally enlarged, as shown in Fig. 11c,d. It can be seen that in the region below the boundary line and near the formed groove bulge, the microstructure of both materials showed a fibrillated fiber texture due to stretching deformation. While in the region above the boundary line near the formed groove bottom, the microstructure of both materials showed a larger density microstructure due to extrusion deformation³⁵. The above experimental phenomena reveal the forming process of material in different regions in mechanical scratching. That is due to the geometric characteristics of the tool's negative front surface and its excessive extrusion, the material above the boundary line near the formed groove bottom outflow is limited and constrained, then the flow rate of the deformation material is slowed down or even stagnant, thus forming a stagnant region. In contrast, the material near the formed groove bulge undergoes a large-displacement shear-slip deformation, thus forming a plastic flow region after passing through the stagnant region edge and the tool's negative front surface.

Microhardness and hardened layer depth analysis

Based on the mechanical scratching experiments described in Sect. "Mechanical scratching experiment", the HVST-1000 microhardness tester was employed to measure the microhardness and hardened layer depth of the formed groove cross-section after scratching the T2 material. Six groups of data were collected at equal intervals from the top to the bottom of the right side of the formed groove. Each group comprised 12 hardness feature points, extending from the groove surface to the interior base material, with the test depth direction approximately perpendicular to the groove surface, as illustrated in Fig. 12. Through several indentation tests, it was determined that when a load of HV0.01 was applied and the spacing between each test hardness point was set at 10 μm, there was no interference between the indentations corresponding to each test hardness point. The microhardness variation curves for the six groups of feature points were obtained from these tests and are presented in Fig. 13.

As can be seen from Fig. 13, the six groups of feature points exhibit a basically consistent trend in microhardness change. Firstly, the microhardness value increases with the depth of the test. Secondly, the microhardness peaks as the test depth increases and reaches a certain value. Finally, as the measurement depth increases

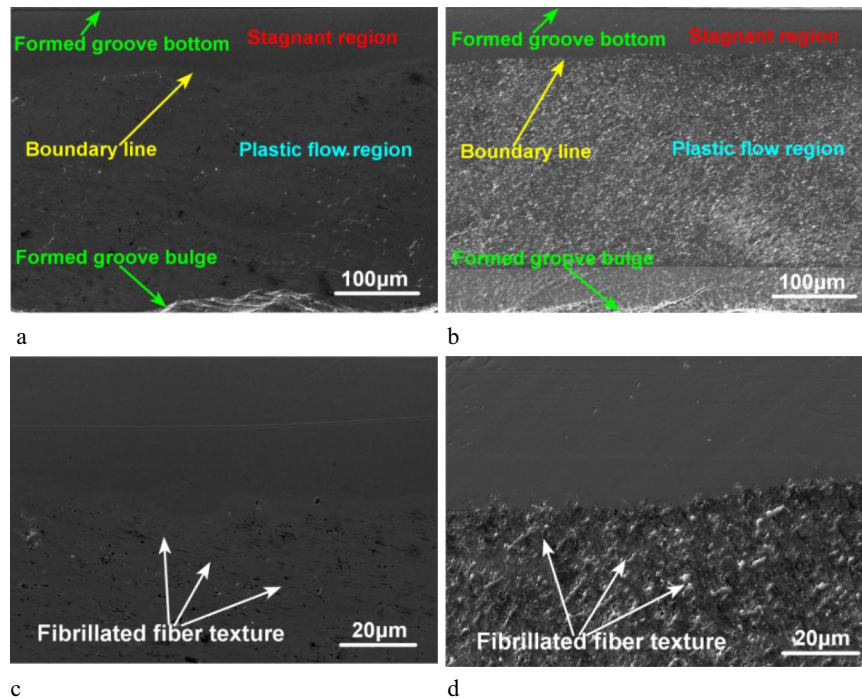


Figure 11. SEM microstructure of the unilateral groove surface in the top view: (a) partitioning phenomenon on the formed groove surface of T2 (b) partitioning phenomenon on the formed groove surface of Al1060 (c) localized enlarged view of the region near the partitioning line of T2 and (d) localized enlarged view of the region near the partitioning line of Al1060.

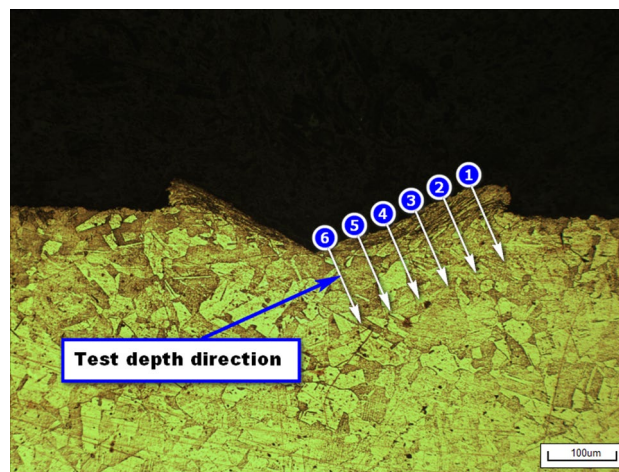


Figure 12. Schematic diagram of measurement microhardness of formed groove cross-section.

further, the microhardness value decreases rapidly and eventually converges to the same stable value, which was measured to be 80.2 HV, approximately equal to the microhardness value of the T2 base material. In summary, the changing trends of the microhardness of each group's feature points with increasing measurement depth are surface hardening, hardness enhancement, and convergence to the hardness of the base material. Comparing the microhardness peak values and the hardened layer depth of the six groups' feature points reveals the following: The microhardness peak values of the 1st and 2nd groups are 145HV and 144HV, respectively, which are approximately 1.79 times the hardness of the base material, with hardened layer depths of 80 μm and 70 μm , respectively. The microhardness peak values of the 3rd and 4th groups are 136HV and 130HV, approximately 1.65 times the hardness of the base material, with hardened layer depths of 60 μm and 50 μm , respectively. The microhardness peak values of the 5th and 6th groups are 124HV and 120HV, respectively, approximately 1.52 times the hardness of the base material, with hardened layer depths of 30 μm and 20 μm , respectively. The above change rule of the six groups' feature points corresponding to the microhardness peak value and the hardened

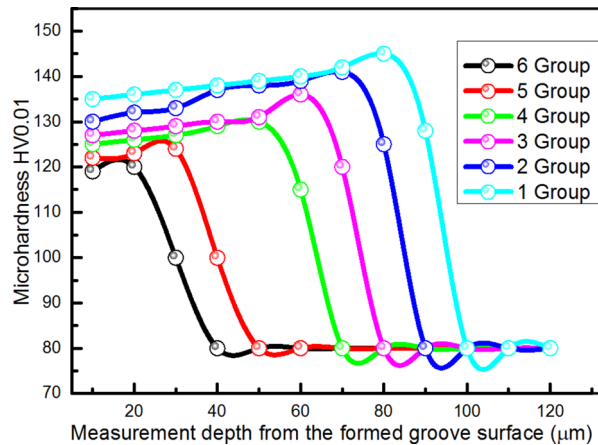


Figure 13. Variation curve of microhardness corresponding to six groups of feature points.

layer depth shows that surface work hardening occurs in the stagnant region at the groove bottom due to the negative front surface geometry of the tool and its over-compacting effect on the material. Meanwhile, due to the large displacement shear-slip deformation of the material in the plastic flow region at the groove top, this accelerates the internal grain movement of the material, resulting in serious dislocation congestion and increased grain slip resistance, which further aggravates the degree of work hardening of the surface layer in this region. Therefore, the surface material in the plastic flow region is more severely work-hardened and strain-enhanced than that in the stagnant region.

Surface roughness analysis

Based on the 3.2 mechanical scratching experiments, the three-dimensional contour and surface roughness of the formed groove surface after mechanically scratching the T2 material were detected and analyzed using the 3D laser confocal microscope LEXT OLS4000. As shown in Fig. 14, six equidistant feature points were selected on the left-formed groove surface for line roughness measurements. The measurement direction for line roughness was parallel to the scratching direction, and the intersection line between the measurement profile and the groove surface corresponded to the line roughness of the feature point. The measured line roughness corresponding to the six feature points of the formed groove surface is presented in Fig. 15.

By comparing the line roughness of the six feature points corresponding to the formed groove surface, it is evident that the line roughness at feature points 1 and 2, located at the top of the groove bulge, are larger at 210 nm and 256 nm, respectively. In the middle of the formed groove, the line roughness at feature point 3 is smaller, measuring 159 nm, while the line roughness at feature point 4 further decreases to 120 nm. At the bottom of the formed groove, the line roughness at feature points 5 and 6 decreases even more and gradually stabilizes at 65 nm and 68 nm, respectively. These results indicate that the roughness values decrease rapidly from the top to the bottom of the groove and then gradually stabilize. This suggests that the stagnant region at the bottom of the groove has lower roughness, whereas the plastic flow region at the top of the groove has higher roughness. The difference in roughness between the top and bottom of the groove surface can be attributed to the distinct forming mechanisms of the material at these regions. The material in the stagnant region at the bottom of the groove undergoes excessive squeezing and restraint by the tool's negative front surface, combined with the good surface finish of the scratching-diamond wedge tool, resulting in reduced surface roughness. Conversely, the material in the plastic flow region at the top of the groove bulge experiences significant tensile deformation due to the excessive extrusion by the tool's negative front surface. Metallographic microstructure analysis reveals that the substantial stretching deformation of the material forms a fibrillated fiber texture arranged in parallel along the same direction. Compared to the denser structure in the stagnant region, the fibrillated fiber texture in the plastic flow region exhibits greater roughness.

Analysis of the evolutionary regularity of the stagnant region

The formed groove bulge height h_B (the highest point of tool-material contact is approximated as the bulge height) and the scratching force $F(x, y, z)$ corresponding to different scratching processing parameters (scratching tool geometry, mounting parameters, scratching speed and materials) were obtained by scratching experiments. By combining with the theoretical calculation model (theoretical calculation model of the geometric parameters of the stagnant region on the formed groove surface), it is possible to determine the absolute value of the working negative rake angle γ_{B0} of the scratching tool, the theoretical values of hydrostatic pressure P_I/k at the point I in the plastic flow plane and the geometric parameters of the stagnant region on the formed groove surface (stagnant region length in plastic flow plane l_{p-sg} , stagnant region length on formed groove surface l_{B-sg} , stagnant region length on formed groove surface in top view l_{V-sg} and the ratio of the stagnant region length on the formed groove surface to the one side length of formed groove in top view Δl_{sg}) can be found. These parameter solutions are used to further investigate the evolution regularity of the stagnant region under the influence of the scratching processing parameters.

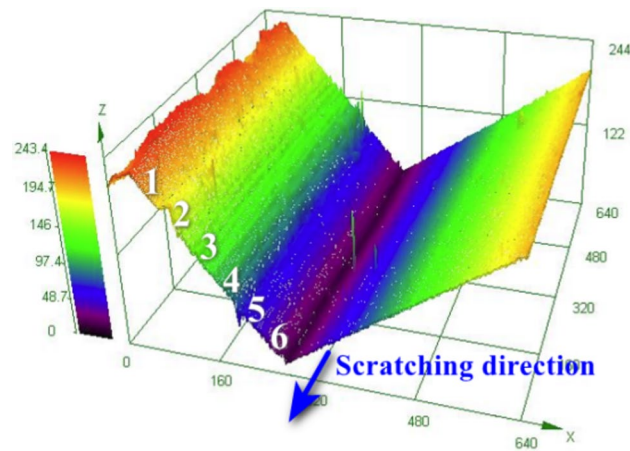


Figure 14. Three-dimensional contour and roughness test points for formed groove surfaces.

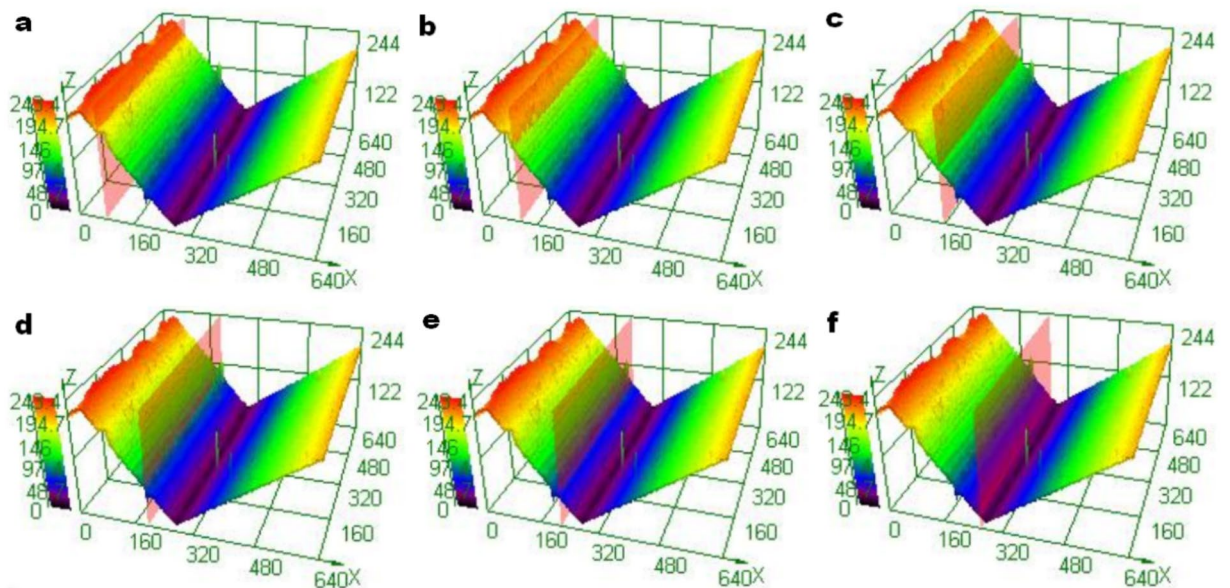


Figure 15. Line roughness value of the six feature points of formed groove surfaces: (a) feature point 1 Ra = 210 nm (b) feature point 2 Ra = 256 nm (c) feature point 3 Ra = 159 nm (d) feature point 4 Ra = 120 nm (e) feature point 5 Ra = 65 nm and (f) feature point 6 Ra = 68 nm.

The effect of scratching tool geometrical parameters on the stagnant region

Combining the experimental parameters with the theoretical calculation model, the geometrical parameters of the stagnant region are solved under the influence of scratching tool geometrical parameters, as shown in Table 3. And the variation curves of the transformation parameters (M1, M2 and M3 solve with reference to the theoretical calculation model) and the geometrical parameters of the stagnant region are plotted, as shown in Fig. 16.

From Fig. 16a–d, it is evident that the length of the stagnant region in the plastic flow plane l_{p-sg} is determined by the hydrostatic pressure P_l/k , and the smaller P_l/k is, the larger the l_{p-sg} will become. According to the theoretical calculation model, it is known that l_{B-sg} is proportional to M_1 with l_{p-sg} and l_{V-sg} is proportional to M2 with l_{p-sg} . M1 is determined by the contact surface normal vectors with the formed groove geometry parameters, and M2 is determined by the contact surface normal vectors, so M1 and M2 will change when the scratching tool geometry parameters change. From Fig. 16b,e, it can be seen that the change rate of l_{p-sg} is greater than that of M1 and M2, so the change rule of l_{B-sg} , l_{V-sg} and l_{p-sg} is consistent under the influence of scratching tool geometric parameters, as shown in Fig. 16c,f. According to the theoretical calculation model, it is also known that Δl_{sg} is proportional to M3 and l_{p-sg} . And M3 is determined by the contact surface normal vector, the formed groove geometric parameters, and the height of the bulge h_B . Therefore, M3 changes drastically when the scratching tool geometry parameters are changed. As shown in Fig. 16b,e, M3 and l_{p-sg} show the same change rule under the influence of scratching tool geometry parameters. Therefore, the change rule of Δl_{sg} and l_{p-sg} is consistent under the influence of scratching tool geometry parameters, as shown in Fig. 16c,f. The above results show that l_{p-sg} is the dominant influencing factor of the geometric parameters of the stagnant region on the formed groove

| Scratching tool's geometric parameters | | \vec{L}_B | γ_{B0} (°) | h_B (μm) | F (x, y, z) (N) | | |
|--|------|----------------------------|-------------------|-----------------|------------------------|------------|-----------------|
| Wedge angle (°) | 80 | (0.0860, -0.9937, -0.0711) | 83.663 | 288 | (0.178,59.005,223.206) | | |
| | 82.5 | (0.0866, -0.9934, -0.0748) | 83.467 | 298 | (0.274,62.779,238.939) | | |
| | 85 | (0.0862, -0.993, -0.0780) | 83.305 | 299 | (0.226,63.881,250.337) | | |
| | 87.5 | (0.0873, -0.9927, -0.0823) | 83.145 | 305 | (0.161,70.752,268.602) | | |
| | 90 | (0.0874, -0.9924, -0.0861) | 82.989 | 310 | (0.250,75.443,280.720) | | |
| Scratching tool's geometric parameters | | $P_{l/k}$ | l_{p-sg} (μm) | l_{B-sg} (μm) | l_{V-sg} (μm) | l_V (μm) | Δl_{sg} |
| Wedge angle (°) | 80 | 3.541 | 767 | 308 | 204 | 327 | 62.39% |
| | 82.5 | 3.59 | 645 | 267 | 173 | 351 | 49.29% |
| | 85 | 3.62 | 591 | 253 | 159 | 371 | 42.86% |
| | 87.5 | 3.714 | 480 | 213 | 130 | 396 | 32.83% |
| | 90 | 3.74 | 448 | 204 | 121 | 420 | 28.81% |
| Scratching tool geometric parameters | | \vec{L}_B | γ_{B0} (°) | h_B (μm) | F (x, y, z) (N) | | |
| Relief angle (°) | 30 | (0.0862, -0.993, -0.0780) | 83.305 | 0.308 | (0.283,75.356,286.903) | | |
| | 32.5 | (0.0862, -0.993, -0.0780) | 83.305 | 0.303 | (0.371,70.302,270.893) | | |
| | 35 | (0.0862, -0.993, -0.0780) | 83.305 | 0.299 | (0.226,63.881,250.337) | | |
| | 37.5 | (0.0862, -0.993, -0.0780) | 83.305 | 0.294 | (0.327,60.663,237.229) | | |
| | 40 | (0.0862, -0.993, -0.0780) | 83.305 | 0.29 | (0.234,57.724,226.944) | | |
| Scratching tool geometric parameters | | $P_{l/k}$ | l_{p-sg} (μm) | l_{B-sg} (μm) | l_{V-sg} (μm) | l_V (μm) | Δl_{sg} |
| Relief angle (°) | 30 | 3.72 | 475 | 209 | 128 | 412 | 31.07% |
| | 32.5 | 3.714 | 482 | 211 | 130 | 389 | 33.42% |
| | 35 | 3.62 | 591 | 253 | 159 | 371 | 42.86% |
| | 37.5 | 3.588 | 641 | 270 | 172 | 355 | 48.45% |
| | 40 | 3.552 | 691 | 287 | 186 | 341 | 54.55% |

Table 3. Theoretical values of the stagnant region geometric parameters corresponding to the scratching tool's geometric parameters.

surface when the scratching tool geometry parameters are changed. Namely, the l_{B-sg} , l_{V-sg} , Δl_{sg} and l_{p-sg} all follow the same pattern of change under the influence of scratching tool geometry parameters.

The effect of scratching tool installation parameters on the stagnant region

Combining the experimental parameters with the theoretical calculation model, the geometrical parameters of the stagnant region are solved under the influence of scratching tool installation parameters, as shown in Table 4. And the variation curves of the transformation parameters and the geometrical parameters of the stagnant region are plotted, as shown in Fig. 17.

From Fig. 17a,d,g, it can be seen that the l_{p-sg} is not only related to P_l/k , but also related to γ_{B0} . The larger γ_{B0} is, the less material flows out of the tool's front surface and thus the larger the l_{p-sg} becomes. When the scratching tool installation parameters are changed, both the contact surface normal vectors and the groove geometry parameters are changed, resulting in a change in M1 and M2 as well. As shown in Fig. 17e, when the absolute value of the rotation angle of the scratching tool around the Y-axis increases, the rate of change of l_{p-sg} is greater than the rate of change of M1 and M2. Therefore, the variation rules of l_{B-sg} , l_{V-sg} and l_{p-sg} are consistent, as shown in Fig. 17f. From Fig. 17b and Fig. 17h, it can be seen that when the rotation angle of the scratching tool around the X-axis and Z-axis increases, the change rate of M1 and M2 is greater than that of l_{p-sg} . This indicates that the contact surface normal vectors and the formed groove geometry parameters both produce substantial changes, which makes M1 and M2 the dominant influences on l_{B-sg} and l_{V-sg} . Therefore, l_{B-sg} and l_{V-sg} are consistent with the change rule of M1 and M2, as shown in Fig. 17c,i. When the scratching tool installation parameters are changed, in addition to the contact surface normal vectors and the formed groove geometry being changed, the height of the formed groove's bulge is also changed, thus leading to a change in M3 as well. From Fig. 17b,e,h, it can be seen that when the scratching tool rotated around the X-axis, Y-axis (forward direction) and Z-axis, with the rotation angle changing M3 and l_{p-sg} appeared the reverse rule of change. By comparison, the change rate of M3 is smaller than that of l_{p-sg} when the scratching tool rotated around the X-axis and Y-axis (forward), therefore the change rule of Δl_{sg} is consistent with that of l_{p-sg} , as shown in Fig. 17c,f. The change rate of M3 is greater than that of l_{p-sg} when the scratching tool rotates around the Z-axis, thus Δl_{sg} follows the same change rule as M3, as shown in Fig. 17i.

The above results show that changes in tool installation parameters can cause substantial changes in the tool's working negative rake angle, contact surface normal vectors, formed groove geometry parameters, and groove rumble height, which would further cause a substantial change in the transformation parameters M1, M2 and M3. The change rate of some transformation parameters even exceeds the change rate of l_{p-sg} when the transformation

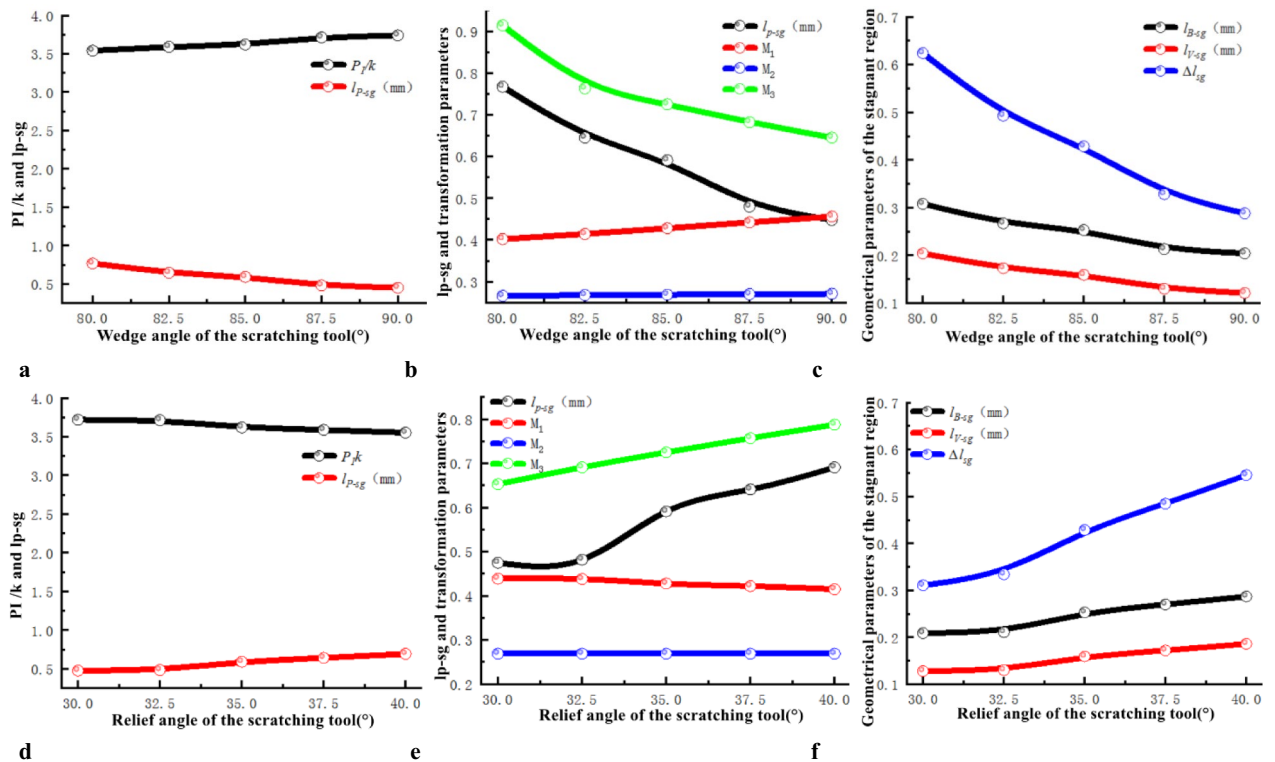


Figure 16. $P_{l/k}$ conversion parameter and geometric parameters of the stagnant region under the influence of the scratching tool geometric parameters: (a) and (d) are the $P_{l/k}$ and l_{p-sg} curve under the influence of scratching tool's geometric parameters (b) and (e) are the l_{p-sg} , M_1 , M_2 and M_3 curve under the influence of Scratching tool's geometric parameters (c) and (f) are the geometric parameters of the stagnant region on the formed groove surface under the influence of scratching tool's geometric parameters.

parameters become the dominant influence on the geometric parameters of the stagnant region on the formed groove surface. As a result, the above analytical results that the change rule of l_{B-sg} and l_{V-sg} is consistent with that of M_1 and M_2 when the scratching tool rotated around the X-axis and Z-axis, as well as the change rule of Δl_{sg} is consistent with that of M_3 when the scratching tool rotated around the Z-axis would be obtained.

The effect of scratching speed and material on the stagnant region

Combining the experimental parameters with the theoretical calculation model, the geometrical parameters of the stagnant region are solved under the influence of scratching speed and material, as shown in Table 5. And the variation curves of the transformation parameters and the geometrical parameters of the stagnant region are plotted, as shown in Fig. 18.

From Fig. 18a,d, it can be seen that γ_{B0} is fixed when the scratching speed and material are changed, and then l_{p-sg} is mainly determined by $P_{l/k}$. The analysis shows that the smaller the scratching speed and the better the plastic adhesion of the material, the smaller the $P_{l/k}$ will become and the larger the l_{p-sg} will become. When the scratching speed and material are changed, the contact surface normal vector and the geometric parameters of the formed groove are unchanged, and M_1 , M_2 are fixed, thus the change rules of l_{B-sg} , l_{V-sg} and l_{p-sg} are consistent, as shown in Fig. 18c,f. When the scratching speed and material are changed, it causes a change in the height of the formed groove bulge h_B , and thus M_3 . From Fig. 18b,e, it can be seen that the smaller the scratching speed is, the better the plastic adhesion of the material is, the larger h_B will become, the smaller M_3 will become, and the change rate of l_{p-sg} is larger than that of M_3 , therefore the change rule of Δl_{sg} is the same as that of l_{p-sg} , as shown in Fig. 18c,f. The above results show that l_{p-sg} is the dominant influencing factor of the geometrical parameters of the stagnant region on the formed groove surface when the scratching speed and material change. Namely, the change rule of l_{B-sg} , l_{V-sg} and Δl_{sg} are consistent with that of l_{p-sg} under the influence of the scratching speed and material.

In summary, l_{p-sg} is the dominant influence of l_{B-sg} , l_{V-sg} and Δl_{sg} when the scratching processing parameters such as scratching tool geometry parameters, rotation angle of the scratching tool around the Y axis, scratching speed, and material are changed. Meanwhile, l_{p-sg} is mainly determined by γ_{B0} with $P_{l/k}$. It is not difficult to conclude from the evolutionary regularity of the stagnant region that γ_{B0} ranges from 82.989° to 83.662° with a small variation when the scratching tool geometric parameters are changed. The working negative rake angle of the scratching tool is a constant value 83.305° , when the rotation angle of the scratching tool is around the Y-axis, the scratching speed and material are changed. Thus $P_{l/k}$ becomes the dominant influence of l_{p-sg} under the influence of scratching tool geometry parameters, rotation angle of the scratching tool around the Y-axis, the scratching speed and material. It can be concretely concluded from the above investigation of the evolutionary regularity of the stagnant region that the smaller the wedge angle of the scratching tool, the larger the relief

| Scratching tool installation parameters | | \vec{L}_B | γ_{B0} (°) | h_B (μm) | F (x, y, z) (N) | | |
|---|------|---------------------------|-------------------|-----------------|---------------------------|------------|-----------------|
| Rotation angle around the X axis (°) | -5 | (0.0434, -0.998, -0.0396) | 86.668 | 248 | (0.326, 60.407, 360.263) | | |
| | -2.5 | (0.0649, -0.996, -0.0590) | 84.964 | 267 | (0.102, 61.082, 278.963) | | |
| | 0 | (0.0862, -0.993, -0.0780) | 83.305 | 299 | (0.226, 63.881, 250.337) | | |
| | 2.5 | (0.107, -0.989, -0.0965) | 81.633 | 311 | (0.0230, 68.561, 254.078) | | |
| | 5 | (0.128, -0.984, -0.116) | 79.97 | 335 | (0.0307, 70.692, 263.001) | | |
| Scratching tool installation parameters | | $P_{I/k}$ | l_{p-sg} (μm) | l_{B-sg} (μm) | l_{V-sg} (μm) | l_V (μm) | Δl_{sg} |
| Rotation angle around the X axis (°) | -5 | 3.541 | 1041.7 | 205 | 142 | 260 | 54.62% |
| | -2.5 | 3.591 | 728 | 224 | 148 | 305 | 48.52% |
| | 0 | 3.62 | 591 | 253 | 159 | 371 | 42.86% |
| | 2.5 | 3.66 | 505 | 287 | 169 | 427 | 39.58% |
| | 5 | 3.704 | 444 | 323 | 176 | 515 | 34.17% |
| Scratching tool installation parameters | | \vec{L}_B | γ_{B0} (°) | h_B (μm) | F (x, y, z) (N) | | |
| Rotation angle around the Y axis (°) | -5 | (0.0862, -0.993, -0.0780) | 83.305 | 308 | (81.002, 72.335, 255.022) | | |
| | -2.5 | (0.0862, -0.993, -0.0780) | 83.305 | 304 | (43.019, 66.115, 251.005) | | |
| | 0 | (0.0862, -0.993, -0.0780) | 83.305 | 299 | (0.226, 63.881, 250.337) | | |
| | 2.5 | (0.0862, -0.993, -0.0780) | 83.305 | 295 | (42.661, 66.702, 251.889) | | |
| | 5 | (0.0862, -0.993, -0.0780) | 83.305 | 291 | (81.605, 72.204, 254.336) | | |
| Scratching tool installation parameters | | $P_{I/k}$ | l_{p-sg} (μm) | l_{B-sg} (μm) | l_{V-sg} (μm) | l_V (μm) | Δl_{sg} |
| Rotation angle around the Y axis (°) | -5 | 3.756 | 434 | 189 | 105 | 460 | 22.83% |
| | -2.5 | 3.652 | 558 | 239 | 141 | 413 | 34.14% |
| | 0 | 3.62 | 591 | 253 | 159 | 371 | 42.86% |
| | 2.5 | 3.652 | 558 | 238 | 150 | 358 | 41.90% |
| | 5 | 3.756 | 434 | 179 | 123 | 309 | 39.81% |
| Scratching tool installation parameters | | \vec{L}_B | γ_{B0} (°) | h_B (μm) | F (x, y, z) (N) | | |
| Rotation angle around the Z axis (°) | -5 | (0.0392, -0.998, -0.0350) | 87.028 | 357 | (27.491, 68.225, 261.385) | | |
| | -2.5 | (0.0633, -0.996, -0.0567) | 85.164 | 327 | (18.567, 66.337, 258.235) | | |
| | 0 | (0.0862, -0.993, -0.0780) | 83.305 | 299 | (0.226, 63.881, 250.337) | | |
| | 2.5 | (0.110, -0.988, -0.100) | 81.451 | 279 | (18.004, 66.369, 255.810) | | |
| | 5 | (0.133, -0.983, -0.122) | 79.605 | 241 | (28.335, 68.544, 260.965) | | |
| Scratching tool installation parameters | | $P_{I/k}$ | l_{p-sg} (μm) | l_{B-sg} (μm) | l_{V-sg} (μm) | l_V (μm) | Δl_{sg} |
| Rotation angle around the Z axis (°) | -5 | 3.62 | 835 | 148 | 103 | 443 | 23.25% |
| | -2.5 | 3.62 | 674 | 202 | 133 | 406 | 32.76% |
| | 0 | 3.62 | 591 | 253 | 159 | 371 | 42.86% |
| | 2.5 | 3.62 | 536 | 301 | 181 | 348 | 52.01% |
| | 5 | 3.62 | 495 | 347 | 200 | 325 | 61.54% |

Table 4. Theoretical values of the stagnant region geometric parameters corresponding to the scratching tool installation parameters.

angle, the smaller the absolute value of the rotation angle of the scratching tool around the Y-axis, the smaller the scratching speed, and the better the plastic adherence of the material, the smaller the P_I/k would become, the larger the l_{p-sg} would become, and then the larger geometric parameters of the stagnant region on the formed groove surface l_{B-sg} , l_{V-sg} and Δl_{sg} would become. On the contrary, the smaller the l_{B-sg} , l_{V-sg} and Δl_{sg} would become.

Deviation analysis of geometric parameters of the stagnant region

Based on the measurement of stagnant region geometric parameters l_{V-sg} and l_V in Sections “Measurement of the experimental values of stagnant region geometric parameters”, the experimental values of l_{V-sg} and l_V corresponding to different scratching processing parameters (scratching tool geometrical parameters, scratching tool installation parameters, scratching speed and material) can be obtained. By combining with the theoretical values of the geometric parameters of the stagnant region on the formed groove surface corresponding to different scratching processing parameters in Sect. “The effect of scratching tool geometrical parameters on the stagnant region” to “The effect of scratching speed and material on the stagnant region”, a comparison can be made between the experimental and theoretical values. This comparison serves to further validate the theoretical calculation model.

The experimental and theoretical values of l_{V-sg} , l_V and Δl_{sg} corresponding to different scratching processing parameters are obtained by measurement extraction, as shown in Table 6 (since l_V is involved in the theoretical calculation, then the experimental and theoretical values of l_{V-sg} and Δl_{sg} would be compared). Comparison can be seen that when the wedge angle increased from 80° to 90°, the experimental and theoretical values of l_{V-sg} and Δl_{sg} show the same change rule of gradual decrease, and their maximum deviations are 12 μm and 3.51%, respectively.

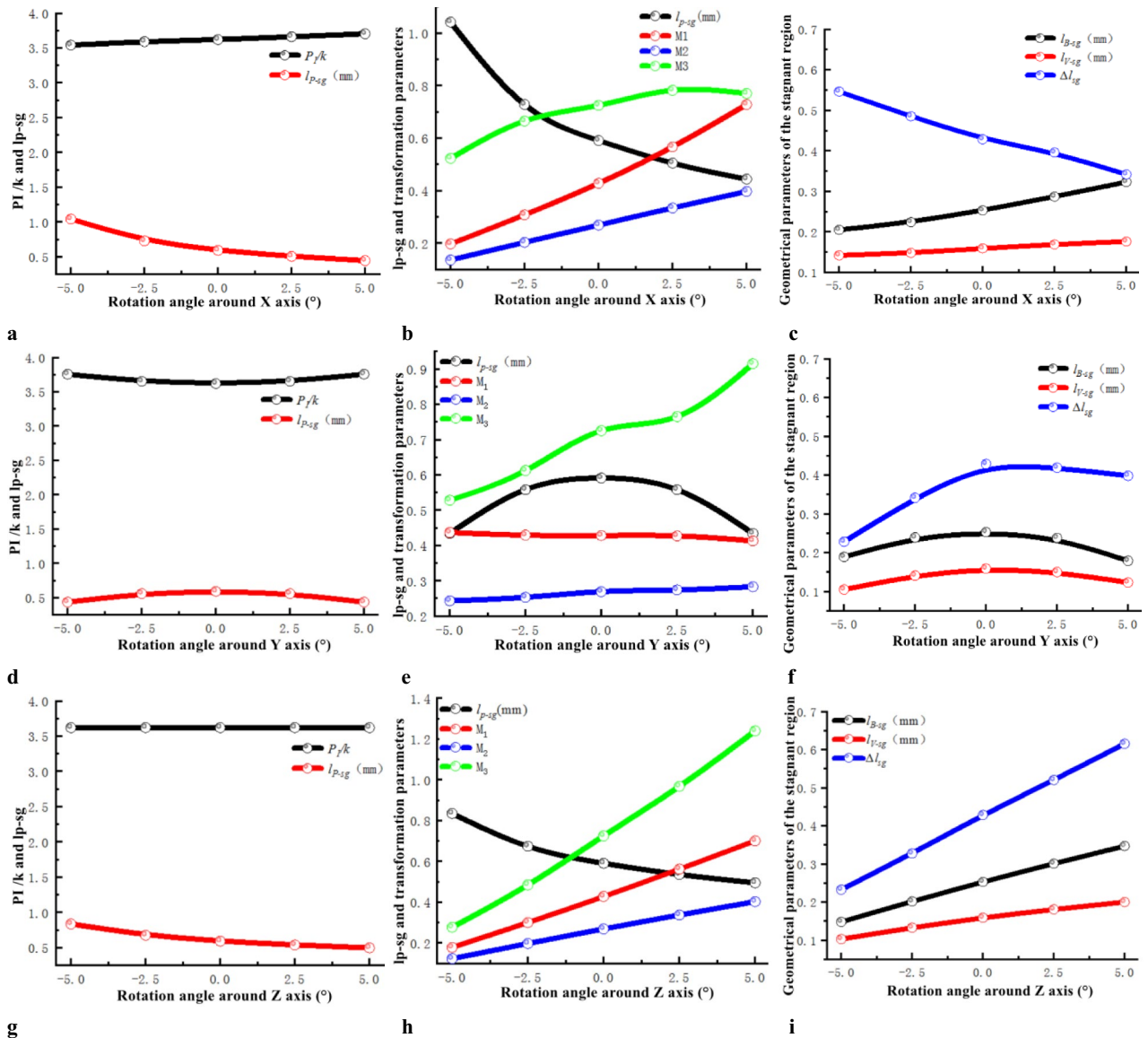


Figure 17. $P_{l/k}$ conversion parameter and geometric parameters of the stagnant region under the influence of the scratching tool installation parameters: (a) (d) and (g) are the $P_{l/k}$ and l_{p-sg} curve corresponding to the rotation angle around the X Y and Z axis, (b) (e) and (h) are the l_{p-sg} and conversion parameter corresponding to the rotation angle around the X Y and Z axis, (c) (f) and (i) are the geometric parameters of the stagnant region corresponding to the rotation angle around the X Y and Z axis.

When the relief angle increased from 30° to 40°, the experimental and theoretical values of l_{V-sg} and Δl_{sg} show the same change rule of gradually increasing, and their maximum deviations are 12 μm and 3.51%, respectively. When the rotation angle of the scratching tool around the X-axis increases from -5° to 5°, the experimental and theoretical values of l_{V-sg} and Δl_{sg} are consistent with a gradual increase, and a gradual decrease, respectively. And their maximum deviations are 13 μm and 4.04%, respectively. When the rotation angle of the scratching tool around the Y-axis increases from 0° to -5°/5°, the experimental and theoretical values of l_{V-sg} and Δl_{sg} show the same change rule of gradual decrease. And their maximum deviations are 12 μm and 3.15%, respectively. When the rotation angle of the scratching tool around the Z-axis increases from -5° to 5°, the experimental and theoretical values of l_{V-sg} and Δl_{sg} show the same change rule of gradual increase. And their maximum deviations are 14 μm and 4.13%, respectively. When the scratching speed increases from 0.1 mm/s to 500 mm/s, the experimental and theoretical values of l_{V-sg} and Δl_{sg} show the same change rule of gradual decrease. And their maximum deviations are 14.4 μm and 3.95%, respectively. When the scratching material T2 and Al1060, the experimental and theoretical values of l_{V-sg} and Δl_{sg} show the same change rule, namely the Al1060 material with better plastic adhesion corresponds to larger values of l_{V-sg} and Δl_{sg} with maximum deviations of 15 μm and 3.67%, respectively.

The above analysis results indicate that, under the influence of different scratching processing parameters, the theoretical and experimental values of l_{V-sg} and Δl_{sg} are basically consistent. Specifically, the larger the scratching tool geometrical parameters, the smaller the scratching tool installation parameters, the smaller the absolute

| Scratching speed and material | | \vec{L}_B | γ_{B0} (°) | h_B (μm) | F (x, y, z) (N) | | |
|-------------------------------|--------|---------------------------|-------------------|-----------------|--------------------------|------------|-----------------|
| Speed (mm/s) | 0.1 | (0.0862, -0.993, -0.0780) | 83.305° | 307 | (0.110, 60.027, 238.926) | | |
| | 1 | (0.0862, -0.993, -0.0780) | 83.305° | 299 | (0.226, 63.881, 250.337) | | |
| | 10 | (0.0862, -0.993, -0.0780) | 83.305° | 282 | (0.230, 68.443, 264.332) | | |
| | 100 | (0.0862, -0.993, -0.0780) | 83.305° | 279 | (0.445, 72.025, 279.661) | | |
| | 500 | (0.0862, -0.993, -0.0780) | 83.305° | 274 | (0.096, 73.308, 282.330) | | |
| Scratching speed and material | | $P_{I/k}$ | l_{p-sg} (μm) | l_{B-sg} (μm) | l_{V-sg} (μm) | l_V (μm) | Δl_{sg} |
| Speed (mm/s) | 0.1 | 3.41 | 855 | 387 | 243 | 381 | 63.78% |
| | 1 | 3.62 | 591 | 253 | 159 | 371 | 42.86% |
| | 10 | 3.75 | 442 | 188 | 118 | 350 | 33.71% |
| | 100 | 3.908 | 275 | 116 | 73 | 346 | 21.10% |
| | 500 | 3.934 | 250 | 106 | 67 | 340 | 19.71% |
| Scratching speed and material | | \vec{L}_B | γ_{B0} (°) | h_B (μm) | F (x, y, z) (N) | | |
| Material | T2 | (0.0862, -0.993, -0.0780) | 83.305° | 0.299 | (0.226, 63.881, 250.337) | | |
| | Al1060 | (0.0862, -0.993, -0.0780) | 83.305° | 0.267 | (0.326, 45.339, 188.625) | | |
| Scratching speed and material | | $P_{I/k}$ | l_{p-sg} (μm) | l_{B-sg} (μm) | l_{V-sg} (μm) | l_V (μm) | Δl_{sg} |
| Material | T2 | 3.62 | 591 | 253 | 159 | 371 | 42.88% |
| | Al1060 | 3.591 | 754 | 320 | 201 | 402 | 50.12% |

Table 5. Theoretical values of the stagnant region geometric parameters corresponding to the scratching speed and material.

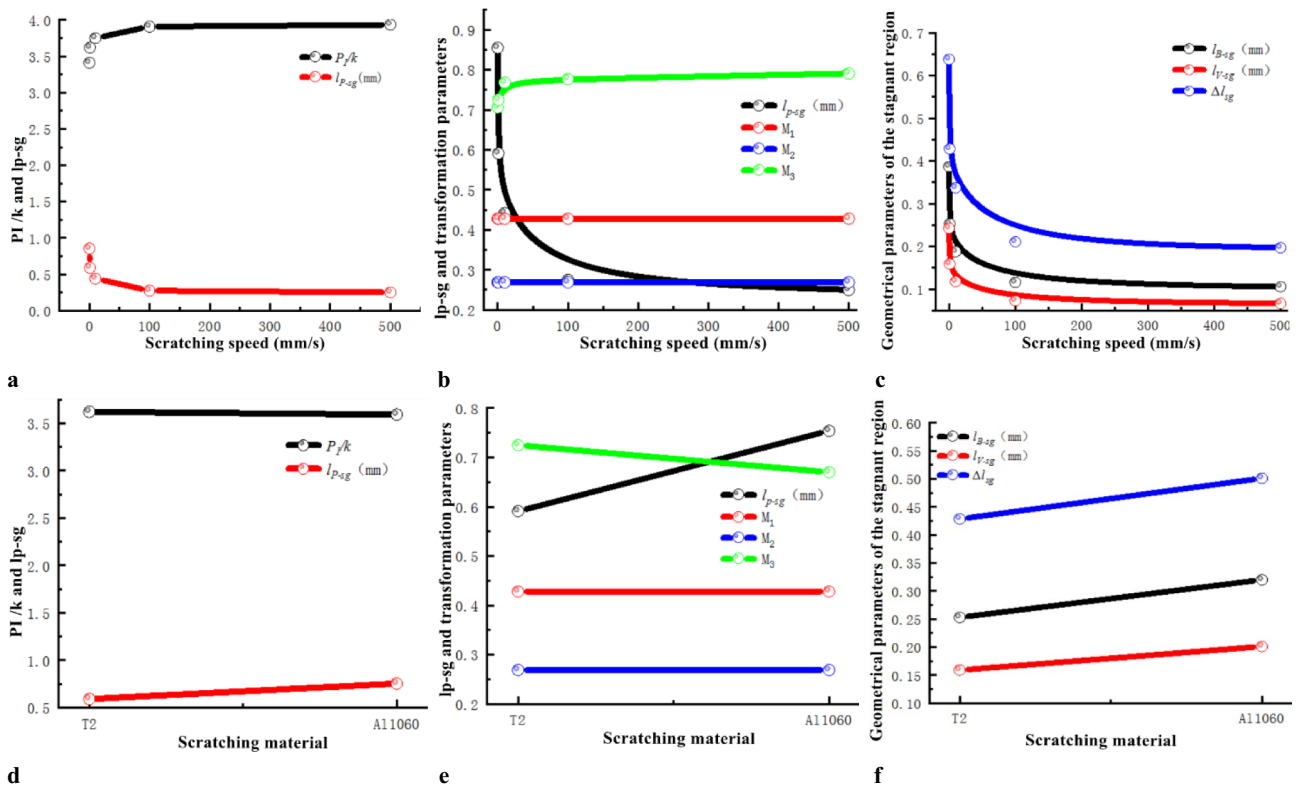


Figure 18. $P_{I/k}$ conversion parameter and geometric parameters of the stagnant region under the influence of the scratching processing factor: (a) and (d) are the $P_{I/k}$ and l_{p-sg} curve corresponding to the scratching speed and material, (b) and (e) are the l_{p-sg} and conversion parameter corresponding to the scratching speed and material, (c) and (f) are the geometric parameters of the stagnant region corresponding to the scratching speed and material.

| Scratching tool's geometric parameters | | l_{V-sg} experimental value (μm) | l_{V-sg} Theoretical value (μm) | l_V (μm) | Δl_{sg} experimental value (%) | Δl_{sg} Theoretical value (%) |
|---|--------|---|--|-------------------------|--|---------------------------------------|
| Wedge angle ($^\circ$) | 80 | 212 | 204 | 335 | 63.28 | 60.90 |
| | 85 | 171 | 159 | 381 | 44.88 | 41.73 |
| | 90 | 130 | 121 | 425 | 30.37 | 28.47 |
| Relief angle ($^\circ$) | 30 | 137 | 128 | 408 | 33.58 | 31.37 |
| | 35 | 171 | 159 | 381 | 44.88 | 41.73 |
| | 40 | 196 | 186 | 347 | 56.48 | 53.60 |
| Scratching tool installation parameters | | l_{V-sg} experimental value (μm) | l_{V-sg} Theoretical value (μm) | l_V (μm) | Δl_{sg} experimental value (%) | Δl_{sg} Theoretical value (%) |
| Rotation angle around the X axis ($^\circ$) | -5 | 153 | 142 | 272 | 56.25 | 52.21 |
| | -2.5 | 157 | 148 | 310 | 50.65 | 47.74 |
| | 0 | 171 | 159 | 381 | 44.88 | 41.73 |
| | 2.5 | 177 | 169 | 430 | 41.16 | 39.30 |
| | 5 | 189 | 176 | 522 | 36.21 | 33.72 |
| Rotation angle around the Y axis ($^\circ$) | -5 | 116 | 105 | 465 | 24.95 | 22.58 |
| | -2.5 | 146 | 141 | 422 | 34.60 | 33.41 |
| | 0 | 171 | 159 | 381 | 44.88 | 41.73 |
| | 2.5 | 160 | 150 | 369 | 43.36 | 40.65 |
| | 5 | 131 | 123 | 320 | 40.94 | 38.44 |
| Rotation angle around the Z axis ($^\circ$) | -5 | 112 | 103 | 411 | 27.25 | 25.06 |
| | -2.5 | 144 | 133 | 408 | 35.29 | 32.60 |
| | 0 | 171 | 159 | 381 | 44.88 | 41.73 |
| | 2.5 | 195 | 181 | 366 | 53.28 | 49.45 |
| | 5 | 214 | 200 | 339 | 63.13 | 59.00 |
| Scratching speed and material | | l_{V-sg} experimental value (μm) | l_{V-sg} Theoretical value (μm) | l_V (μm) | Δl_{sg} experimental value (%) | Δl_{sg} Theoretical value (%) |
| Speed s(mm/s) | 0.1 | 254 | 243 | 392 | 64.80 | 61.99 |
| | 1 | 171 | 159 | 381 | 44.88 | 41.73 |
| | 10 | 127 | 118 | 365 | 34.79 | 32.33 |
| | 100 | 87.4 | 73 | 365 | 24.55 | 20.00 |
| | 500 | 79.9 | 67 | 350 | 22.83 | 19.14 |
| material | T2 | 171 | 159 | 381 | 44.88 | 41.73 |
| | Al1060 | 216 | 201 | 409 | 52.81 | 49.14 |

Table 6. Experimental and theoretical values of l_{V-sg} , l_V and Δl_{sg} corresponding to different mechanical scratching processing parameters.

value of the rotation angle of the scratching tool around the Y-axis, the smaller the scratching speed, and the better the plastic adhesion of the material, the larger the l_{V-sg} and Δl_{sg} become. The maximum deviation value are 15 μm for l_{V-sg} and 4.13% for Δl_{sg} , respectively. The above deviation analysis results first verified the theoretical calculation model of the stagnant region geometric parameters on the formed groove surface. Secondly, they provides the theoretical and experimental basis for effectively controlling the size of the stagnant region on the formed groove surface.

Conclusion

This paper establishes a theoretical calculation model for the stagnant region on the formed groove surface, analyzes the forming process, characteristics, and evolutionary regularity of the stagnant region, and subsequently reveals the forming mechanism of the stagnant region in mechanical scratching from three perspectives: theory, simulation, and experimentation. The specific conclusions are as follows:

1. A theoretical calculating model of the geometric parameters of the stagnant region on the formed groove surface is established based on the mechanism of contact friction partitioning and the slip-line field theory. The theoretical calculating model shows that the geometrical parameters of the stagnant region on the formed groove l_{B-sg} , l_{V-sg} and Δl_{sg} are determined by the stagnant region length in the plastic flow plane l_{p-sg} and the transformation parameters (M1, M2 and M3).
2. The formation process of the stagnant region in the scratching process was explored by simulation of orthogonal cutting with a negative rake angle tool. The result show that the stagnant region is not the product of the forming process such as cold welding or pressure fusion, but a plastic deformation region formed due to the geometrical characteristics of the negative front surface of the scratching tool and its excessive extrusion acting on the material, leading to the formation of an adhesive friction within the material.

3. Through the study of stagnant region characterization, it is concluded that the material of the stagnant region at the groove bottom is subjected to the excessive extrusion by a high-finish scratching tool, while the material of the plastic flow region near the groove bulge undergoes a large-displacement shear-slip deformation. Consequently, compared with the material in the plastic flow region, the metallographic organization of the material in the stagnant region is finer and denser, the surface hardening peak and the hardened layer depth are smaller, and the surface roughness is significantly better.
4. The analysis of the evolutionary regularity of stagnant region shows that the smaller the wedge angle of the scratching tool, the larger the relief angle, the smaller the absolute value of the rotation angle of the scratching tool around the Y-axis, the smaller the scratching speed, and the better the plastic adherence of the material, the smaller the P_r/k become, the larger the l_{p-sg} become, and consequently, the larger geometric parameters of the stagnant region on the formed groove surface l_{B-sg} , l_{V-sg} and Δl_{sg} would become. Deviation analysis of the geometric parameters of the stagnant region shows that the change pattern of the theoretical and experimental values of l_{V-sg} and Δl_{sg} are basically consistent, with a maximum deviation value of 15 μm and 4.13%, respectively. This verifies the theoretical calculation model.

Data availability

The datasets used or analyzed during the current study are available from the corresponding author on reasonable request.

Received: 28 January 2024; Accepted: 29 July 2024

Published online: 02 August 2024

References

1. Ding, Y., Shi, G. & Zhang, H. Research on the plastic flow characteristics of metal material in mechanical scratching. *Int. J. Adv. Manuf. Technol.* **115**, 1171–1185 (2021).
2. Ding, Y. C., Shi, G. F. & Guoquan, S. Analysis of the stagnant characteristics of the material in the mechanical ruling process. *J. Mech. Eng.* **54**(19), 182 (2018).
3. Ohbuchi, Y. & Obikawa, T. Finite Element Modeling of Chip Formation in the Domain of Negative Rake Angle Cutting. *J. Eng. Mater. Technol.* **125**(3), 324–332 (2003).
4. Ozturk, S. & Altan, E. Position of the separation point in machining with a rounded-edge tool. *Proc. Inst. Mech. Eng. Part B J. Eng. Manuf.* **227**(7), 965–971 (2013).
5. Abebe, M. *A Slip-Line Solution for Negative Rake Angle Cutting* (Manufacturing Engineering Transactions, 1981).
6. Lee, E. H. & Shaffer, B. W. The theory of plasticity applied to a problem of machining. *J. Appl. Mech.* **18**(4), 405–413 (1951).
7. Fang, N. Tool-chip friction in machining with a large negative rake angle tool. *Wear* **258**(5–6), 890–897 (2005).
8. Ozturk, S. & Altan, E. Slip-line metal cutting model with negative rake angle. *J. Brazil. Soc. Mech. Sci. Eng.* **34**(3), 246–252 (2012).
9. Ozturk, S. & Altan, E. A slip-line approach to the machining with rounded-edge tool. *Int. J. Adv. Manuf. Technol.* **63**(5–8), 513–522 (2012).
10. Zhang, H. T., Liu, P. D. & Hu, R. S. A three-zone model and solution of shear angle in orthogonal machining. *Wear* **143**(1), 29–43 (1991).
11. Uysal, A. & Altan, E. A new slip-line field modeling of orthogonal machining with a rounded-edge worn cutting tool. *Mach. Sci. Technol.* **18**(3), 386–423 (2014).
12. Kita, Y., Ido, M. & Tuji, Y. The influence of the cutting speed on the mechanism of metal removal by an abrasive tool. *Wear* **71**(1), 55–63 (1981).
13. Wan, L. *Numerical Analysis of Metal Cutting Process* (Mechanical Engineering Shanghai University, 2016).
14. Weule, H., Huntrup, V. & Tritschle, H. Micro-cutting of steel to meet new requirements in miniaturization. *CIRP Ann.* **50**(1), 61–66 (2001).
15. Usui, E. & Makino, R. An example of stress and strain distributions in slow speed, steady-state machining. *J. Jpn. Soc. Precis. Eng.* **33**(387), 245–251 (1967).
16. Kountanya, R. K. & Endres, W. J. A high-magnification experimental study of orthogonal cutting with edge-honed tools. *ASME Proc. ASME Manuf. Eng. Division ASME Int. Mech. Eng. Congress Expos.* **12**, 157–164 (2001).
17. Wan, L. & Wang, D. Z. Numerical analysis of the formation of the dead metal zone with different tools in orthogonal cutting. Simulation modelling practice and theory. *Int. J. Feder. Eur. Simul. Soc.* **56**, 1–15 (2015).
18. Komanduri, R. Some aspects of machining with negative rake tools simulating grinding. *Int. J. Mach. Tool Design Res.* **11**(3), 223–233 (1971).
19. Ozturk, S. Slip-line modeline of machining and determine the influence of rake angle on the cutting force. *Trans. Can. Soc. Mech. Eng.* **36**(1), 23–35 (2011).
20. Anilchandra, A. R. & Surappa, M. K. Influence of tool rake angle on the quality of pure magnesium chip-consolidated product. *J. Mater. Process. Technol.* **210**(3), 423–428 (2010).
21. Hoshi, K. On the metal cutting mechanism with the built-up edge. *Hokkaido Univ. Faculty Eng. Memoirs* **12**(3), 241–271 (1960).
22. Agmell, M., Ahadi, A., Gutnichenko, O. & Jan, E. S. The influence of tool micro-geometry on stress distribution in turning operations of AISI 4140 by FE analysis. *Int. J. Adv. Manuf. Technol.* **89**(912), 1–14 (2016).
23. Guo, Y. B., Anurag, S. & Jawahir, I. S. A novel hybrid predictive model and validation of unique hook-shaped residual. *CIRP Annals Manuf. Technol.* **5**(1), 81–84 (2009).
24. Armarego, E. J. A. & Herath, A. B. Predictive models for machining with multi-edge form tools based on a generalized cutting approach. *CIRP Annals Manuf. Technol.* **49**(1), 25–30 (2000).
25. Jiang, W. P. *Research on Design Method of Long-Life Diamond Ruling Tool of Diffraction Grating* (Changchun University of Science and Technology, 2012).
26. Zhong, C. S. & Han, J. T. *Fundamentals of Calculation of Plastic Deformation Forces in Metals* (Metallurgical Industry Press, 1994).
27. Zhang, P. *Basic Theory and Analytical Application of Elastic-Plastic Mechanics* (Harbin Institute of Technology Press, 2014).
28. Qiu, Q. Y. *Modern Metal Cutting Technology* (China Machine Press, 1994).
29. Kara, F., Aslantas, K. & Çiçek, A. Prediction of cutting temperature in orthogonal machining of AISI316L using artificial neural network. *Appl. Soft Comput.* **38**, 64–74 (2016).
30. Kara, F., Aslantas, K. & Çiçek, A. ANN and multiple regression method-based modelling of cutting forces in orthogonal machining of AISI 316L stainless steel. *Neural Comput. Appl.* **26**, 237–250 (2015).

31. Wan, L., Wang, D. Z. & Gao, Y. The investigation of mechanism of serrated chip formation under different cutting speeds. *Int. J. Adv. Manuf. Technol.* **82**(5–8), 951–959 (2016).
32. Shi, G., Liu, J., Zhang, Y., & Shi, G. Laser diffraction application on detection technology of online tool setting. International Conference on Optoelectronics & Microelectronics IEEE (ICOM) 62–64 (2016).
33. Ding, Y., Shi, G., Zhang, H., Shi, G. & Han, D. Analysis of critical negative rake angle and friction characteristics in orthogonal cutting of AL1060 and T2. *Sci. Progress* **103**(1), 0036850419878065 (2020).
34. Ding, Y. C., Shi, G. F., Luo, X. H. & Shi, G. Q. Study on the critical negative rake angle of the negative rake angle tool based on the stagnant characteristics in micro-cutting. *Int. J. Adv. Manuf. Technol.* **107**(5–6), 2055–2064 (2020).
35. Cui, Z. Q. *Metallography and Heat Treatment* (China Machine Press, 2020).

Acknowledgements

The authors would like to thank the anonymous reviewers for their valuable comments and suggestions which helped us improve the content quality and presentation of this paper.

Author contributions

Y.D.: Investigation, theoretical analysis, validation, writing—original draft. W.Y.: Theoretical modelling. G.S.: Conceptualization, supervision, project administration. H.H.: Investigation, validation, writing—review and editing. J.W.: Investigation, validation, writing—review and editing. L.M.: Experiment and testing. G.L.: Experiment and testing. The authors claim that they agree to publish.

Funding

The authors would like to acknowledge the Natural Science Foundation of China (NSFC) (Grant No. 51405031, No. 51575057, No. 51075042 and No. 52375405), the Science and Technology Project of Jilin Province (No. 20180414068GH, 20190302123GX), the Project of Jilin Provincial Department of Education (No. JJKH20230293KJ), and the Doctoral Initiation Programme (No. 2023005). The authors also thank the anonymous reviewers for their valuable comments.

Competing interests

The authors declare no competing interests.

Additional information

Correspondence and requests for materials should be addressed to Y.D. or G.S.

Reprints and permissions information is available at www.nature.com/reprints.

Publisher's note Springer Nature remains neutral with regard to jurisdictional claims in published maps and institutional affiliations.

Open Access This article is licensed under a Creative Commons Attribution-NonCommercial-NoDerivatives 4.0 International License, which permits any non-commercial use, sharing, distribution and reproduction in any medium or format, as long as you give appropriate credit to the original author(s) and the source, provide a link to the Creative Commons licence, and indicate if you modified the licensed material. You do not have permission under this licence to share adapted material derived from this article or parts of it. The images or other third party material in this article are included in the article's Creative Commons licence, unless indicated otherwise in a credit line to the material. If material is not included in the article's Creative Commons licence and your intended use is not permitted by statutory regulation or exceeds the permitted use, you will need to obtain permission directly from the copyright holder. To view a copy of this licence, visit <http://creativecommons.org/licenses/by-nc-nd/4.0/>.

© The Author(s) 2024